DROPLET FORMATION ON DEMAND AT A MICROFLUIDIC T-JUNCTION

by

Kelly Min He

B.A.Sc, The University of British Columbia, 2011

A THESIS SUBMITTED IN PARTIAL FULFILLMENT OF

THE REQUIREMENTS FOR THE DEGREE OF

MASTER OF APPLIED SCIENCE

in

THE FACULTY OF GRADUATE and POSTDOCTORAL STUDIES

(Electrical and Computer Engineering)

THE UNIVERSITY OF BRITISH COLUMBIA

(Vancouver)

February 2015

Abstract

Microfluidic aliquot dispensing technologies have been utilized in many chemical or biological high throughput assays to provide high-speed deposition of high-resolution droplets. Particularly, these aliquots can be used to dispense a controlled volume of liquid into multi-well plates in drug screening applications. However, existing platforms are often designed to print a limited set of materials where each material is handled by an independently actuated nozzle. A more convenient and scalable technology that could allow digital output of multiple materials on demand must be explored.

Monodispered droplets can be formed continuously in a microfluidic T-junction when two input flows of immiscible fluids are maintained. However, it is difficult to form stable air separated aliquots in a simple T-junction configuration. Electrowetting-on-dielectric (EWOD) is commonly used to control individual droplets in a planar configuration. But it is not usually used in microfluidic channels. In this device, a new method for creating air separated aliquots on demand using EWOD at a microfluidic T-junction was demonstrated. Since air is the carrier fluid, these aliquots can be dispensed without further liquid processing. A device that consists of SU-8 channels with electrodes in alignment with the channels was designed and fabricated. A double wedged junction was incorporated at the dispersed channel to create a barrier pressure that allows the meniscus location to be controlled by the applied pressures. Droplets of approximately 15 nL can be generated by applying a voltage at the electrode at the junction. Liquid flow is stopped when the voltage is removed. This mechanism can be used as a digital valve to generate a sequence of aliquots of different materials for a multi-material printing platform.

Preface

The concept of the aliquot-on-demand system was developed by me in collaboration with Ali Ahmadi under the supervision of Dr. Boris Stoeber and Dr. Konrad Walus. I designed and fabricated the devices used in the experiments. I planned and conducted all the experimental work and data analysis.

Table of contents

List of tables

List of figures

Acknowledgements

I would like to thank all my colleagues at UBC for offering help, inspiration, and encouragement whenever I need them.

I would like to thank my advisors, Dr. Boris Stoeber and Dr. Konrad Walus, for their hard work that earned me the opportunity to do this research. They have given me unlimited support and encouragement during my studies. Thank you for always asking critical questions and keep pushing me to try to do better. Doing research work has pushed me to think critically and ask questions that I would have never thought of before.

I would like to thank my parent for their unconditional love and support.

Dedication

This thesis is dedicated to my parents who taught me the value of hard work and persistence.

Chapter 1: Introduction

1.1 Objective and motivation

In recent years, inkjet droplet dispensing technologies that have been used in commercial printers for many years have been combined with microfluidic technologies to dispense microdrops that can be utilized in new applications including DNA synthesis [1], drug discovery [2], and precise electronics fabrication [3]. State of the art microdrop (commonly referred to as aliquots) dispensing technologies have the advantage of being able to dispense high-resolution isolated aliquots with controlled sizes in the range of nanoliters or picoliters on demand. This allows precise control of material deposition at high-speed, making it a suitable candidate for high-throughput applications [4]. Particularly, these microfluidic aliquot generation systems have been used for dispensing controlled volumes of liquid into high throughput screening multi-well plates for drug discovery applications [5], [6]. In most existing multi-material platforms, input materials are prepared in advance and then supplied to the system where liquid processing on demand is not possible. Also, different materials are usually dispensed by independently actuated nozzles, making it necessary to have a complex actuation system when processing multiple materials [2], [7], [8].

The objective of this project is to design and fabricate a microfluidic system that can generate a sequence of controllable aliquots of different materials to be used in a lab-on-a-printer printing platform. A scalable device that can sequentially deliver droplets of different materials is especially important in applications that involve a large variety of reagents such as chemical synthesis or screening processes [9], [10]. The lab-on-a-printer concept is illustrated in Figure 1.

Unlike conventional inkjet systems that only dispense predetermined materials, it incorporates conventional microfluidic processing submodules to allow fluid processing at the printer on demand. The processed materials are then passed to a multi-material output valve module where an output sequence of material can be specified and dispensed through one nozzle.

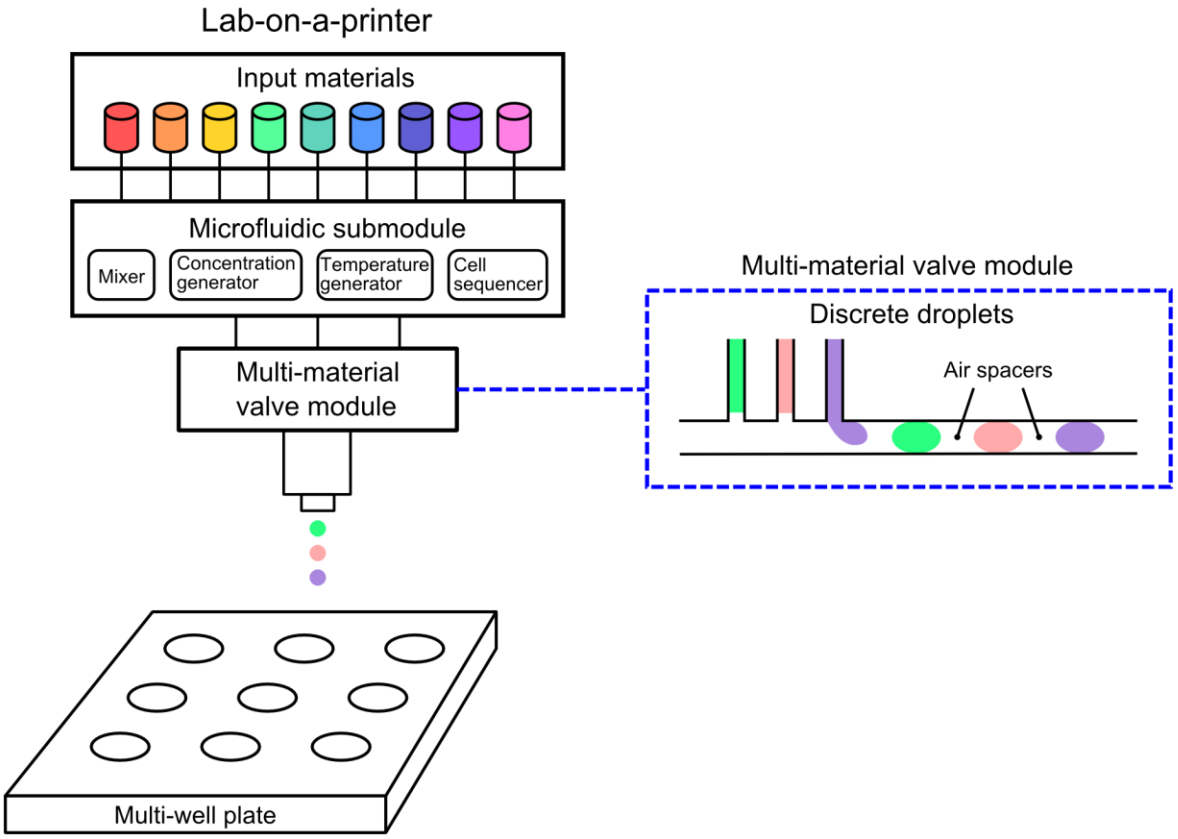

Figure 1: Lab-on-a-printer schematic with a multi-material valve module that can generate a sequence of air separated aliquots of different materials on demand

There is a wide variety of available mechanical microvalves that can provide precise microfluidic control using actuation methods including electrical, magnetic, piezoelectric, and pneumatic [11], [12]. Using these mechanical microvalves, liquid segments of different materials can be formed [6], [13]. However, each input will require a separate pair of valve and actuator.

Since many of the existing mechanical valve mechanisms require complicated fabrication, a system with many materials could result in a very complicated structure. Also, a carrier liquid is usually needed to form a stable flow. Instead of using mechanical valves, the purpose of the proposed design is to develop a new digital valve mechanism that could output a sequence of discrete droplets of different materials. For this application, the aliquots must be completely separated by air so that they can be dispensed without further liquid processing to remove the carrier fluid. Also, air spacers can limit cross contamination and are especially important in applications where individual properties between droplets must be conserved [14]. The proposed design combines a conventional continuous T-junction aliquot formation technique with electrowetting-on-dielectric (EWOD) actuation to provide controlled droplet formation on demand. This design is scalable and is suitable to be used in a platform involving multiple materials.

1.2 Multiphase T-junction droplet formation

The T-junction is one of the most commonly used structures for continuous monodispersed droplet and bubble formation [15]–[17]. In this configuration, as illustrated in Figure 2, two immiscible fluids merge at a T-shaped junction at constant flow rates. One of the input channels and its extension that is used for transporting the produced aliquot is usually referred to as the carrier channel and the part that is perpendicular to the carrier channel is usually referred to as the dispersed channel.

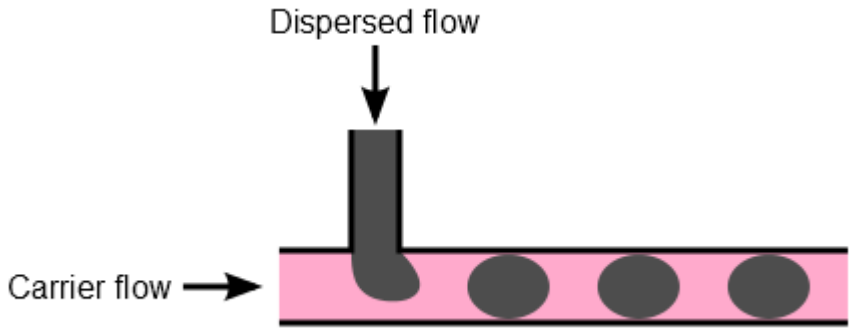

Figure 2: Droplet breakup in a T-junction

The flow behavior of a two phase flow can be predicted by the Capillary number of the carrier flow

$$Ca = \frac{\mu u}{\gamma}, \qquad (1)$$

where μ is the viscosity of the carrier fluid, u is the flow rate of the carrier fluid, and γ is the interfacial tension. In a flow where the capillary number is small, typically $Ca < 0.1$, interfacial tension dominates shear stress and the flow operates in the squeezing regime and the liquid is cut off close to the junction. The squeezing regime is usually the desired operation regime for aliquots formed in this manner. At high Ca a laminar flow is formed in the carrier channel before breakup could happen further away from the junction [15]. In the squeezing regime, as the fluid in the dispersed channel flows into the carrier flow, the pressure difference across the part of the fluid that is in the carrier flow builds up and eventually this pressure difference breaks the fluid off from the fluid remaining in the dispersed channel, forming a droplet or a bubble. Droplet or bubble sizes, frequencies, and flow regimes are dependent on channel geometry and the flow rates of the different phases and these properties cannot be individually tuned without causing

changes to other properties [15], [18]. Highly monodispersed droplets or bubbles can be formed continuously when the flow rates of the two materials are maintained [16], [19].

There are three possible phase distributions between the two immiscible fluids in a T-junction system in square channels. The phase distributions of flows with two immiscible liquids, gas-liquid with hydrophilic walls, and gas-liquid with hydrophobic walls are illustrated in Figure 3.

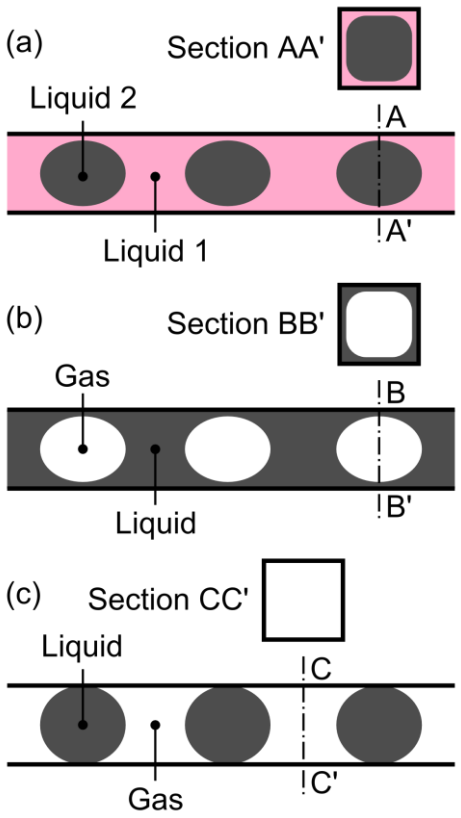

Figure 3: Possible phase distribution in a T-junction system with square channels

(a) liquid-liquid (b) gas-liquid with hydrophilic walls (c) gas-liquid with hydrophobic walls

In a liquid-liquid flow (Figure 3 (a)), one liquid forms a thin film along the walls and corners of the channel, wrapping around droplets of the other liquid. In a gas-liquid system with

hydrophilic walls (Figure 3 (b)), the liquid would wrap around gas slugs, providing a lubricating film to carry the gas slugs across the channel smoothly. In a gas-liquid system with hydrophobic walls (Figure 3 (c)), liquid droplets are completely separated by the gas phase [20]. However, due to the lack of the lubricating liquid layer along the channel walls, droplets formed in a fully hydrophobic system are not stable and could result in significant variations in droplet size and shapes during droplet formation or resulting from merging during transport along the channel [14], [21]. In a hydrophilic gas-liquid system with circular channels, the connecting liquid film thickness is significantly thinner than that in square channels. However circular channels are difficult to fabricate and they are not compatible with many existing microfluidic fabrication and integration methods [14]. In many applications that incorporate the gas-liquid T-junction system, the gas is used as the dispersed fluid with a hydrophilic carrier fluid. The gas bubbles can act as spacers to promote mixing within the individual droplets [5], [22], [23]. But this configuration is not suitable for our application where we want to output a series of droplets of different materials in an air carrier flow.

1.3 Electrowetting-on-dielectric

The electrowetting effect is the electromechanical effect of change in wettability of a surface by a liquid due to the presence of an electric field. Electrowetting-on-dielectric (EWOD) is the configuration where a dielectric layer separates the liquid from at least one of the electrodes to enable a higher electric field and a wider variety of possible liquids [24]–[28]. As illustrated in Figure 4, when the voltage is applied across the dielectric layer with a conductive liquid above the layer, charge is accumulated at the surface of the solid-liquid interface, causing the surface energy to decrease, hence reducing the apparent contact angle of the liquid from θ_0 to θ. A

hydrophobic layer is usually deposited on the dielectric to minimize hysteresis and improve device operation [24], [25], [28], [29].

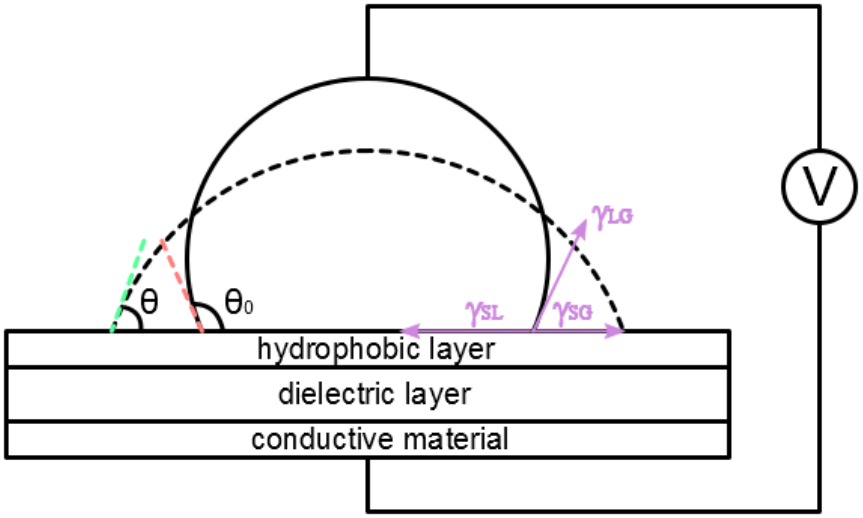

Figure 4: EWOD mechanism

In fact, the local contact angel θ_0 at the liquid-solid-gas interface remains unchanged. But that effect is only visible at a very small length scale (in the scale of hundreds of nanometers) at the contact line and has negligible effect on the overall surface energy representation of the liquid. The electric field causes a significant change to the curvature of the liquid-gas interface near the contact line leading to the apparent contact angle θ [27]–[29].

As shown in Figure 4, the contact angle of a liquid is determined by the balance between the three interfacial tension energies and it is expressed by the Young's equation,

$$\gamma_{SL} = \gamma_{SG} - \gamma_{LG} \cos\theta_0, \quad (2)$$

where γ_{SL} is the solid-liquid interfacial tension, γ_{SG} is the solid-gas interfacial tension, γ_{LG} is the liquid-gas interfacial tension, and θ is the contact angle. The effect of the electric field can be

modeled through an effective solid-liquid interfacial tension caused by an applied voltage as described by Lippmann's equation,

$$\gamma_{SL}(V) = \gamma_{SL,0} - \frac{1}{2} cV^2, \quad (3)$$

where $\gamma_{SL,0}$ is the solid-liquid interfacial tension when there is no voltage applied, c is the total capacitance per unit area of the dielectric layer, and V is the applied voltage (V_{rms} is used when AC voltage is applied). By combining equations (2) and (3) we get the governing equation of EWOD that is known as the Lippmann-Young's equation [24], [26], [28], [30],

$$\cos\theta(V) = \cos\ \theta_0 + \frac{1}{2\gamma_{LG}} cV^2, \quad (4)$$

where $\theta(V)$ is the contact angle as a function of applied voltage.

EWOD is commonly used to manipulate discrete droplets to perform tasks including creating an individual droplet from a reservoir, transporting, mixing and splitting a droplet. It allows complex fluid operations to be controlled by electrical signals alone for a wide range of droplet-medium combinations [28], [31], making it an ideal technology for lab on a chip devices. Devices are usually configured with liquid sandwiched between a transparent conductive top plate and a bottom plate patterned with a desired grid of electrodes covered with a dielectric layer. The plates are usually separated by a spacer and held together but not bonded together. A hydrophobic layer is usually coated on both plates to improve performance. Some example applications with this configuration include chips for dried blood spot analysis [32], glucose detection [33], droplet based automated algal culture condition screening [34], multi-material bio-assay [35], and material detection using capacitance [36].

1.4 Related work

The proposed device combines a pressure driven T-junction configuration with EWOD actuation to control droplet formation at the junction. Some devices with concepts similar to the proposed design have been made. Morishita *et al.* have fabricated a trench structure with electrodes on three sides using shadowmask evaporation and demonstrated they were able to move liquid forward using EWOD. However, the group did not attempt droplet breakup [37]. Jenkins *et al.* have generated a pressure change by actuating droplets with EWOD in a sealed channel. Up to 6 droplets and a maximum pressure of 7.6 kPa was formed by actuating water droplets in an oil medium, proving that is it possible to create a pressure change using EWOD on droplets [38]. Malloggi *et al.* have shown that they were able to control the droplet size and formation frequency at a liquid-liquid flow focusing junction by applying a voltage to the electrode at the junction. The device was fabricated by clamping PDMS channels onto a glass slide coated with ITO and Teflon. They did not attempt forming droplets in air [18].

As mentioned before, droplets formed in a hydrophobic environment using a conventional T-junction mechanism are completely separated by air but are not stable. Oskooei *et al.* have fabricated a flow rate driven T-junction chip that is hydrophilic at the junction and hydrophobic elsewhere. Gas plugs are formed in a stable manner at the hydrophilic junction and as the flow reaches the hydrophobic part the liquid transitions into discrete slugs and continues to flow downstream. Droplets formed in this manner were stable and completely disconnected by air. Similar to conventional T-junction mechanisms, droplets are formed continuously when the flow rates are maintained [14]. In our proposed device, the liquid aliquots are formed in a hydrophilic

environment using a combination of EWOD and hydrodynamic forces and transported to a channel with hydrophobic and hydrophilic surfaces.

1.5 Design overview

As shown in Figure 5, the proposed design has multiple dispersed junctions with different materials connected to one carrier channel. The two pressure sources are maintained at constant pressures and the electrodes are actuated to form droplets.

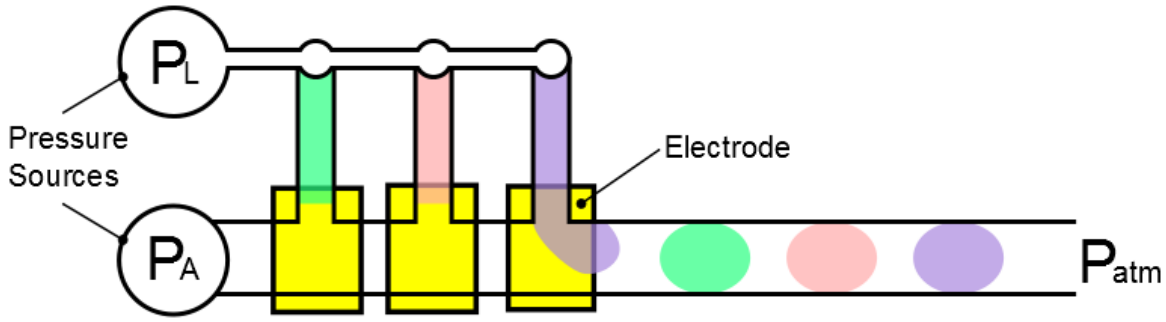

Figure 5: Design overview

The pressure difference across a curved interface of two phases is described by the Laplace pressure equation:

$$P_1 - P_2 = \gamma_{12}(\frac{1}{R_1} + \frac{1}{R_2}) \quad (5)$$

where R_1 and R_2 are the two principle radii of curvature of the surface. The applied pressures are maintained at a level such that when the electrode is turned off, the liquid stops near the junction. As shown in Figure 6, when the electrode underneath the T-junction is actuated, the contact angle between the liquid and the dielectric layer above the electrode decreases, causing the pressure required to maintain at the same point to decrease. As a result, liquid will move forward

and break into droplets due to the hydrodynamic forces from the continuous flow in the carrier channel. In this design, only two applied pressures maintained at constant levels are required to handle multiple materials, and only electrical signals are required to actuate the aliquot formation and control the formation frequency.

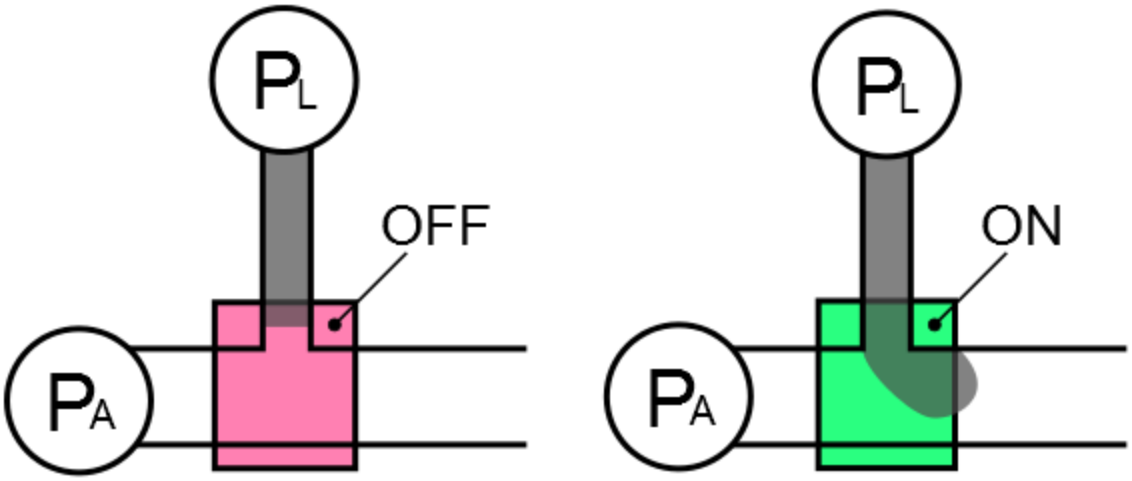

Figure 6: EWOD actuated droplet breakup at a T-junction

In the conventional T-junction configuration, constant flow rates are driving the materials. And in a constant flow rate liquid-gas system the gas is usually placed in the dispersed flow. In our configuration the gas is the carrier flow and constant pressures are driving the materials.

Chapter 2: Fabrication

We have designed a fabrication procedure that is similar to typical parallel plate EWOD configuration but with channels in between that are aligned with electrodes. The fabrication steps are illustrated in Figure 7.

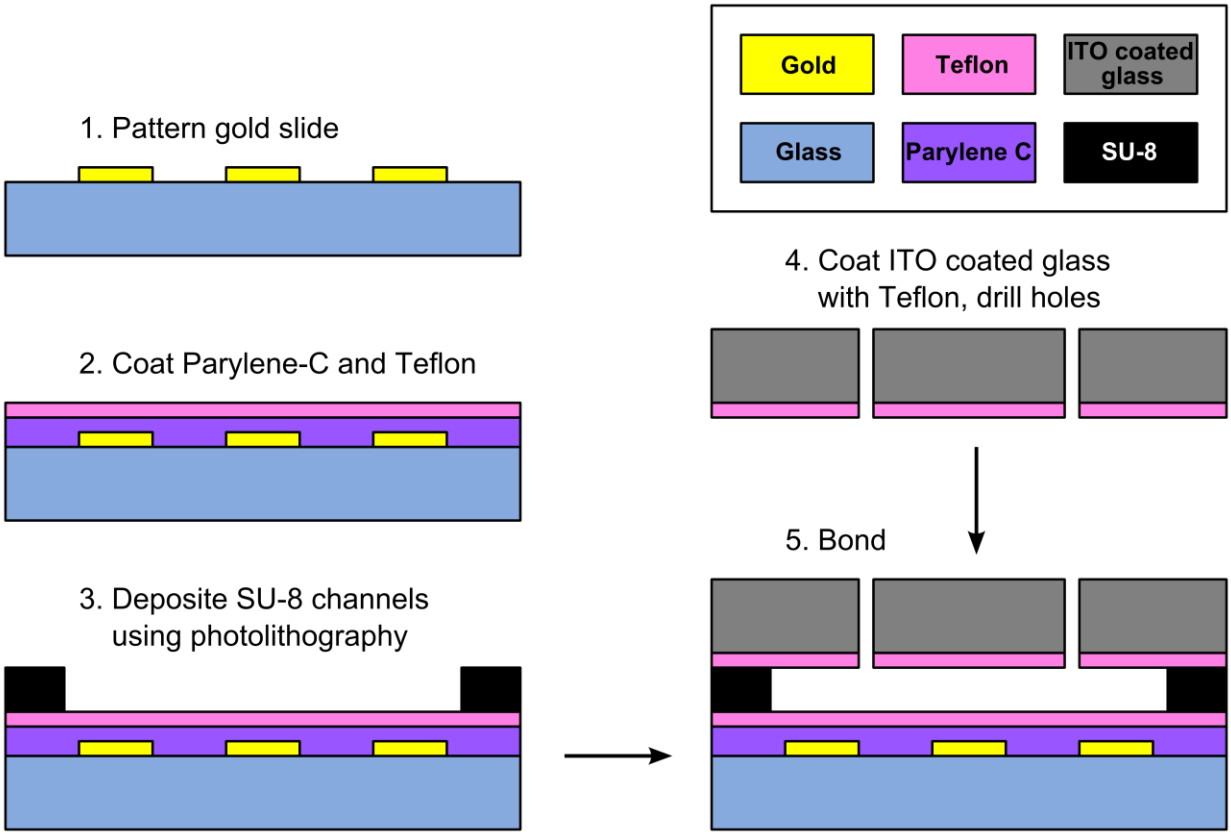

Figure 7: Fabrication flow chart

1. **Pattern electrodes**

   Microscope slides (25 mm by 75 mm by 1mm) coated with 50 angstroms of chromium followed by 1000 angstroms of gold are purchased from EMF Corporation (Rochester, New York). The metal coating on these slides is patterned to form the desired electrode

patterns by shielding wanted parts with a positive photoresist (Shipley 1813, Microchem, Westborough, Massachusetts) and immersing the slides into gold and then chromium etchants to remove the metal from unwanted areas. The fabrication steps and parameters for photoresist are listed in Table 1

Table 1: Shipley 1813 fabrication parameters

Step	***Parameters***
Spin photoresist (Shipley 1813)	4700 rpm, 45 s, acceleration at 23 rpm/s
Soft bake	15 minutes at 80 °C Cool down to room temperature on a flat surface
Exposure	8 seconds at 8.5 mW/cm^2
Develop	In MF319 developer for 3-5 minutes or until pattern is clear
Plasma clean (Trion PECVD)	Pressure: 200 mTorr Power: 70 W O_2: 70 sccm Temperature: 20 °C Time: 20 s
Post exposure bake	20 minutes at 120 °C

Potassium iodide gold etchant is mixed using $I_2/KI/H_2O$ with the ratio of 1:4:40. Chromium etchant (Chromium Etchant 1020) is purchased from Transene Company, Inc.

(Danvers, Massachusetts). In both processes, etching is performed using the following steps:

1. Immerse slide into etchant for 15 seconds
2. Remove slide from etchant and rinse with DI water
3. Dry slide with compressed air
4. Check under microscope and if there are still gold/chromium left immerse into etchant for 10 seconds and go to step 2

Both etchant can be recycled and reused until etch rate is too slow.

After etching the photoresist is removed with oxygen plasma for 5 minutes in a Trion PECVD system (pressure: 200 mTorr, power: 150 W, O_2: 70 sccm, temperature: 20 °C).

2. Coat patterned slides with Parylene-C and Teflon

The patterned slides are then coated with Parylene-C by vapour deposition. The dimer and the coating device are both from Specialty Coating Systems (Indianapolis, Indiana). Before coating Parylene-C, the surfaces are treated with an adhesion promoter A174 Silane (also from Specialty Coating Systems, Indianapolis, Indiana) using a standard immersion procedure with the following steps:

1. Prepare a solution by mixing 500 ml of DI water, 500 ml of of IPA and 10 ml of A174 Silane in a beaker with a stirrer for at least 5 hours
2. Cover electrodes with Kapton tape
3. Immerse slides in IPA for 5 minutes
4. Immerse slides into water/IPA/A174 mixture for 30 minutes

5. Dry slides by placing them upright for 30 minutes (do not dry with compressed air)
6. Immerse slides into IPA for 10 minutes
7. Dry slides with compressed air
8. Bake slides at 110 °C for 10 minutes

Parylene adhesion is significantly improved with the adhesion promoter. The Kapton tape is removed and replaced with new tape before coating the slides with Parylene-C. Parylene-C is conformally coated onto the slides using a vapour deposition method. A wide range of thickness of Parylene-C can be coated by this method and the thickness can be controlled by controlling the weight of the dimer that is used in a given process run. In this device 5-6 μm of Parylene-C is the target deposition thickness. The Kapton tape is peeled off to reveal the electrode contacts following Parylene deposition. It is possible to coat Parylene onto the slides without using the adhesion promoter but due to the weak adhesion to the slides, the Parylene covering the working area of the device may be peeled off with the tape.

The Parylene-C layers are annealed at 300 °C for 3 hours in a vacuum chamber with a small nitrogen flow. It was shown that Parylene-C annealed this way is a better insulator without causing any changes to its chemical structure [39]. But this must be done in an oxygen-free environment because Parylene-C can oxidize at a temperature above 120 °C [39], [40]. Parylene annealing is done in a PECVD system from Trion with the following steps:

1. Place slides into the chamber and form a vacuum
2. Flush the chamber with nitrogen

3. Form a vacuum again, repeat steps 2 and 3 twice
4. Set a small nitrogen flow (10 sccm)
5. Set temperature to 300 degrees, it will take about 30 minutes to reach 300 degrees
6. Maintain system at 300 degrees for 3 hours
7. Set temperature to room temperature, it will take about one hour to reach room temperature

Teflon-AF 2400 (DuPont Canada, Mississauga, Ontario) is then spin coated onto the Parylene layer at 1000 rpm for 45 seconds. The resulting film thickness is measured to be in the range of 100-200 nm using a Tencor AlphaStep 200 Profiler.

3. Deposit SU-8 channels using photolithography

Channels are built and aligned with the electrodes using negative photoresist SU-8 3050 (MicroChem, Westborough, Massachusetts) and photolithography. The grey layer in Figure 8 is the SU-8 mask and the pink layer is the mask for the electrodes. The area on the image that is not grey within the grey rectangle is the footprint of the resulting SU-8 structure after lithography.

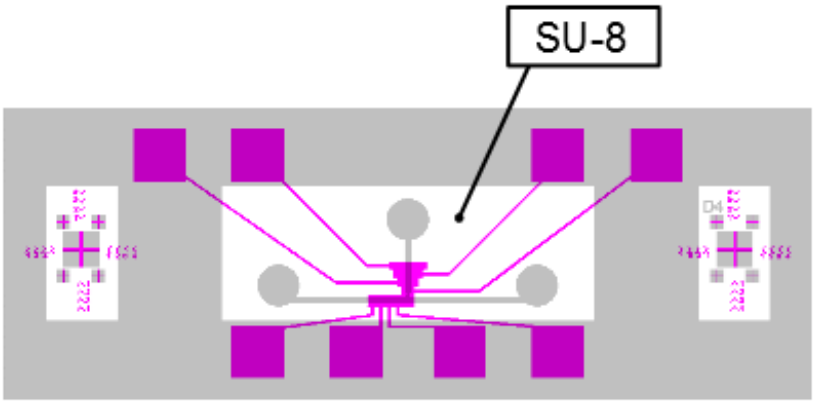

Figure 8: SU-8 channel and electrode structures

Before spin coating SU-8, the Teflon coated surface is treated with weak oxygen plasma for 10 seconds in a Trion PECVD system (pressure: 200 mTorr, power: 50 W, O_2: 70 sccm, temperature: 20 °C) with a piece of PDMS covering the channel area to remove the Teflon at the outer rim. If SU-8 is spun directly onto a Teflon coated surface, the hydrophobicity of the surface will cause the SU-8 to coil towards the center of the surface during soft bake. Treating the outer edge of the slide with oxygen plasma will expose the hydrophilic glass and as a result the SU-8 layer will be pinned down at the edge even though the center is hydrophobic. Any openings in the hydrophobic part will otherwise cause the SU-8 to coil towards the hydrophilic part of the slide. The fabrication steps for the SU-8 channels are listed in Table 2.

Table 2: SU-8 3050 fabrication parameters

Step	***Parameters***
Spin photoresist	Step 1: 500 rpm, 10 s, acceleration at 100 rpm/s Step 2: 1000 rpm, 30 s, acceleration at 300 rpm/s Step 3: 0 rpm, 10 s, deceleration at 300 rpm/s
Soft bake	1 minute at 65 °C 35 minutes at 95 °C Cool down to room temperature on a flat surface
Exposure	43 seconds at 8.5 mW/cm^2
Post exposure bake	1 minute at 65 °C 3 minutes at 80 °C

Hot plates are leveled before baking to minimize thickness variation. Most SU-8 fabrication parameters are selected based on the recommended values provided by MicroChem. Exposure time and hard bake parameters are purposely reduced so that the SU-8 is not completely annealed to allow bonding. The resulting thickness of the SU-8 channel layer is around 80-90 μm (measured with Tencor AlphaStep 200 Profiler). The channel height is assumed to be 85 μm for all the calculations in the rest of this thesis.

4. Coat ITO with Teflon and drill holes

The ITO coated slides (700 nm thick ITO coating, 8-12 ohms/square sheet resistance, purchased from SPI supplies, West Chester, Pennsylvania) are cut into 14 mm by 65 mm pieces and inlet holes with a 1.8 mm diameter are drilled using a micro milling platform. Teflon is then spun coated onto the drilled slides at 1000 rpm for 45 seconds, resulting in a film with thickness around 100 to 200 nm. The film is annealed at 240 °C for 15 minutes right after spinning. Figure 9 shows the location of the ITO top plate in the device.

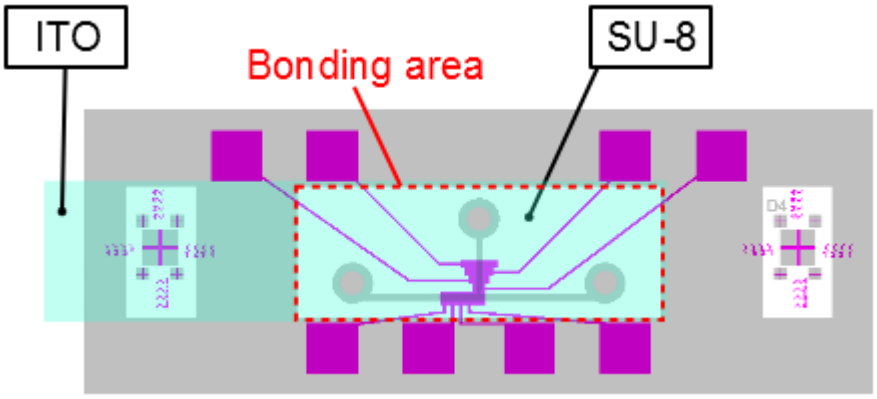

Figure 9: ITO top plate

5. Bonding

The top plate is bonded onto the SU-8 channels by applying a pressure at an elevated temperature to allow partially crosslinked SU-8 to adhere to the Teflon top plate. SU-8 is an epoxy based photoresist and it has been shown that SU-8 microfluidic channels can be sealed with glass by applying a pressure to SU-8 heated above its glass transition temperature [41]. In order to have a successful bond, the SU-8 must be crosslinked sufficient to maintain the channel structure when the pressure is applied during bonding and must have sufficient partially crosslinked polymer chains to allow bonding to the Teflon-coated ITO slides. Also, sufficient pressure must be applied to the sample to allow bonding but without cracking the glass. Most importantly a close contact between the two surfaces must be maintained for bonding to be successful. Suitable parameters were determined through successive trials.

The glass transition temperature is 50-65 °C for uncrosslinked SU-8 and 150-240 °C for crosslinked SU-8 [41]. To determine a working bonding temperature, bonding was attempted at various values between the glass transition temperatures of uncrosslinked and crosslinked SU-8. Through experiments, combining the SU-8 annealing procedure described earlier, bonding at 80 °C for 30 minutes can give completely bonded channels that maintain the intended geometry of design.

To achieve this bonding, we have built a clamp using standard optomechanical parts. Images of the clamp are shown in Figure 10. As shown on the images, the chip is placed between two pieces of 5/8 inch thick glass and clamped together and tightened by screwing the two screws into the pillars on the two sides. The heights from the top rod to the bottom of the clamp on each side (as indicated by the arrow in Figure 10) are measured and matched using a caliper to ensure the flatness of the clamp.

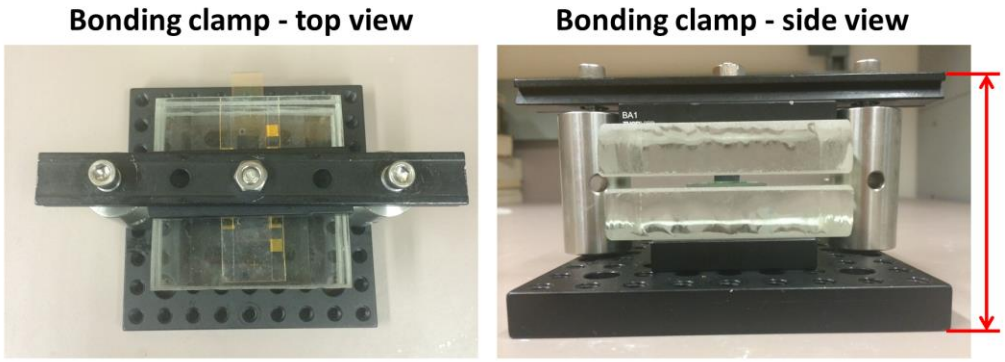

Figure 10: Bonding clamp

A piece of rubber that is 2 mm thick is placed above the ITO at the bonding area, as shown in Figure 11, to provide an even force distribution to the SU-8 while reducing the risk of cracking the top plate.

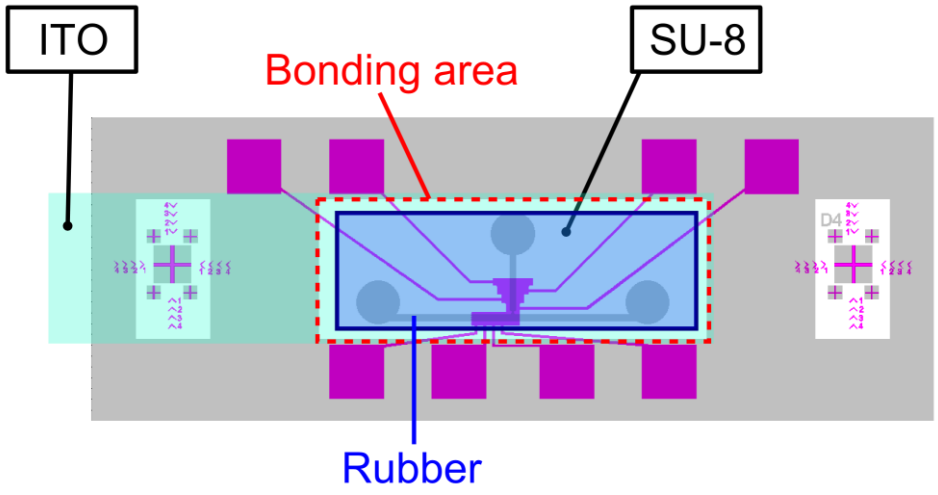

Figure 11: Bonding configuration

All the parts of the bonder, including the rubber, are preheated at 80 °C in the oven for at least 30 minutes before bonding.

After bonding, pipette tips are glued onto the inlets by epoxy to act as ports for tubings. Epoxy is also applied to the outer edge of the top plate to secure the bonding. If not glued together the top plate can be easily ripped off after bonding. But with epoxy applied bonded channels shown little sign of leakage after many experiments. Figure 12 is an image of a device fabricated with the procedures described.

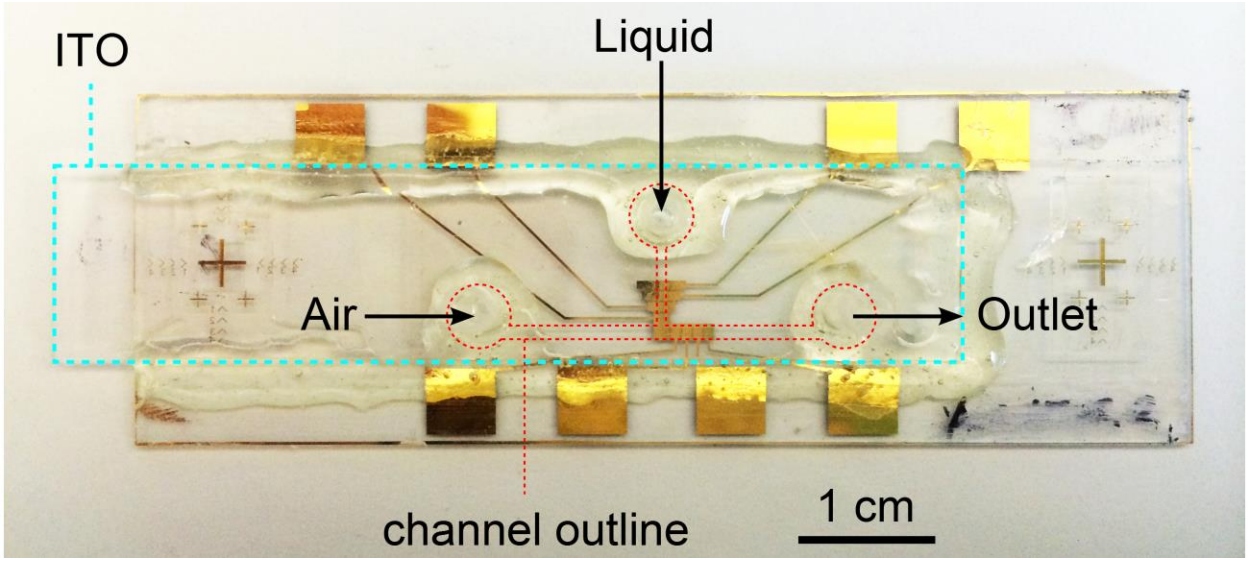

Figure 12: Image of a device fabricated with the procedure described in this chapter

Chapter 3: Channel design and characterization

For this device, we need to fabricate channels in a T-junction such that we can easily stop liquid near the junction and be able to move the liquid into the carrier channel using EWOD. The ideal design would be one that can stop the liquid a little behind the junction with a reasonable range of working pressure so that cross contamination can be limited in a chip with multiple junctions. In our channels, the vertical channel walls are hydrophilic (SU-8) and the top and bottom walls are hydrophobic (Teflon).

3.1 Straight channels

Straight channels are used in conventional pressure T-junction. The liquid interfaces in a straight channel with Teflon top and bottom walls and SU-8 side walls are illustrated in Figure 13.

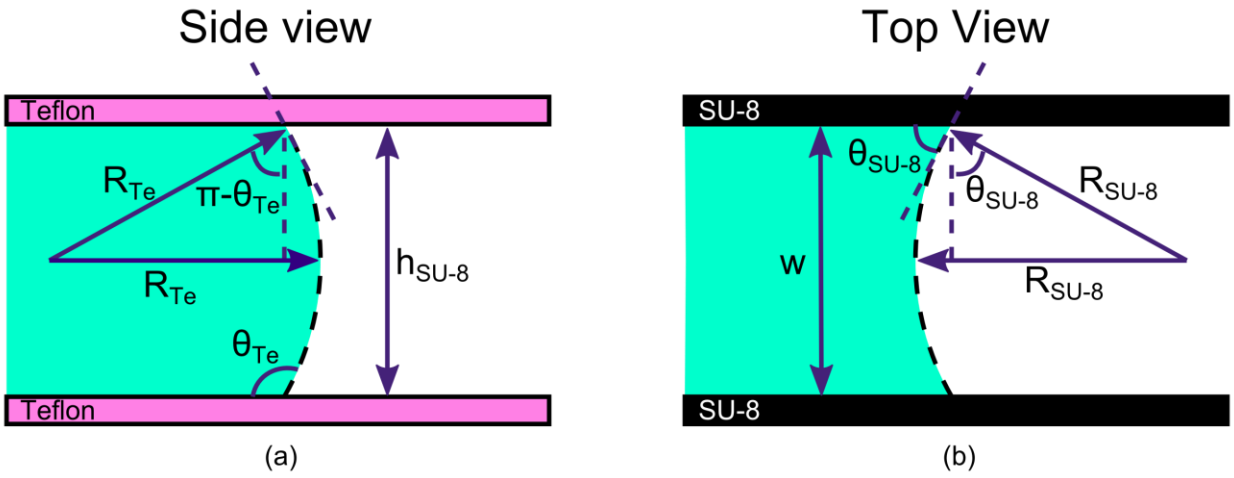

Figure 13: Liquid interface from the (a) side view (b) top view

Figure 13 (a) is the side view profile of the liquid forming a convex shape with hydrophobic contact angles with a radius of curvature (R_{Te}) of

$$R_{Te} = \frac{h_{SU-8}}{|2\cos(\theta_{Te})|}, \quad (6)$$

where h_{SU-8} is the height of the SU-8 channels and θ_{Te} is the static contact angle of Teflon. Figure 13 (b) is the profile of the liquid from the top view of the chip forming a concave shape due to the hydrophilic surfaces of SU-8. The radius of curvature of the meniscus in contact with the SU-8 channel walls (R_{SU-8}) is

$$R_{SU-8} = \frac{w}{|2\cos(\theta_{SU-8})|}, \quad (7)$$

where w is the width of the SU-8 channels and θ_{SU-8} is the static contact angle of SU-8. The Laplace pressure across the liquid interface is

$$\Delta P = \gamma_{lg}\left(\frac{1}{R_{Te}} + \frac{1}{R_{SU-8}}\right) = \gamma_{lg}\left(\frac{|2\cos(\theta_{Te})|}{h_{SU-8}} - \frac{|2\cos(\theta_{SU-8})|}{w}\right). \quad (8)$$

In a straight channel where w is constant, the Laplace pressure across the gas-liquid interface is constant and does not vary with the location of the meniscus. As a result it is very difficult to stop liquid in a straight channel in a well-defined location using different applied pressures and it is not possible to stop liquid before the junction. Wedged junctions were designed to solve these problems.

3.2 Wedged junction

A double wedged junction for the dispersed channel shown in Figure 14 was designed as it allows for stopping the fluid in a well-defined location using pressure control. Since the structure is not straight, as the liquid flows towards the junction, the Laplace pressure across the gas-liquid interface changes. The variables describing this geometry are defined in Figure 14. The parameters must be selected such that an increasing amount of pressure will be required as the

liquid moves toward the junction. This increasing pressure will act as a pressure barrier that will stop/start liquid flow as the electrode is turned off/on.

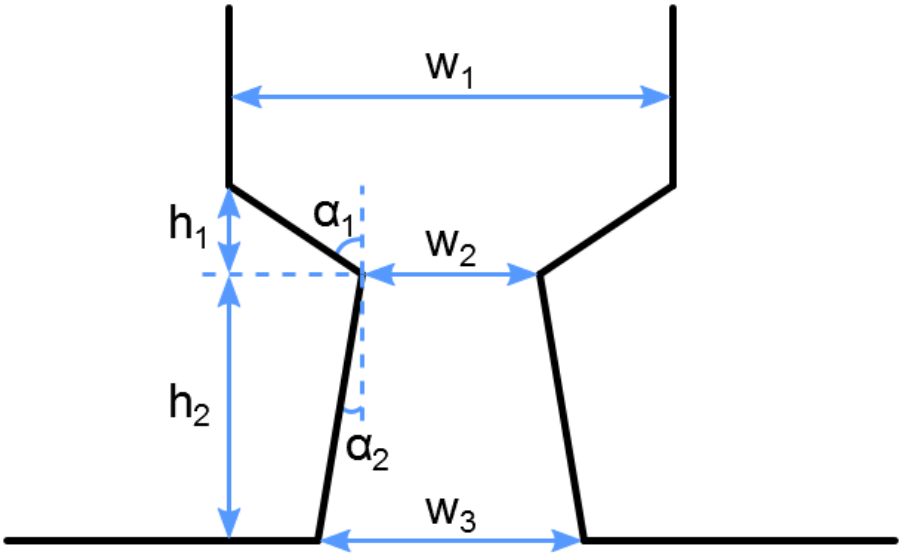

Figure 14: Wedged juntion design

In the expanding part of the channel with a length of h_2, as shown in Figure 15, if the sum of the static contact angle of SU-8 and the angle of expansion of the channel ($\theta_{su\text{-}8} + \alpha_2$) is smaller than 90°, the meniscus will form a concave shape as it moves forward. With this shape an increasing pressure will be required as the liquid moves forward. The static contact angle of the SU-8 used in this device was measured to be 73°-78° on a flat SU-8 surface (by using a contact angle tool, Attension Theta, to measure contact angle on droplets deposited on SU-8 surfaces) and 55°-75° in SU-8 channels (by taking images of liquid at rest in straight SU-8 channels and finding the tangents to the liquid interfaces). To ensure $\theta_{su\text{-}8} + \alpha_2$ is always less than 90° while maximizing the wedged effect, α_2 was designed to be slightly less than 10°. A contracting part was added before the expanding part so that the width of the straight channel is not limited by w_2. Having

channels that are too narrow between the fluid reservoir and the junction can result in high flow resistance or cause fabrication problems.

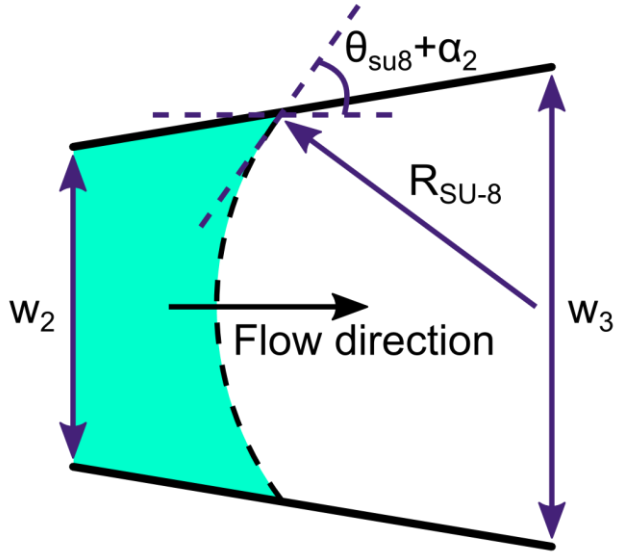

Figure 15: Flow in the expanding part

3.3 Liquid interface profiles

The liquid profile from the side view remains constant as in Figure 13 (a) because the top and bottom plates are parallel. As the liquid moves into the wedged part of the channel, the radius curvature equation changes due to the geometry change. The liquid profile in a contracting channel is illustrated in Figure 16. Because SU-8 is a hydrophilic material, $\theta_{SU\text{-}8}$-α_1 is always smaller than 90°, as a result the liquid will always form a concave shape.

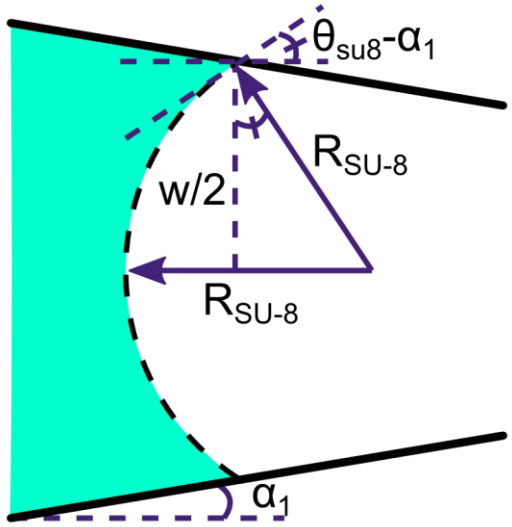

Figure 16: Liquid profile in a contracting channel

The radius of curvature in this region is

$$R_{SU-8} = \frac{w}{|2\cos(\theta_{SU-8} - \alpha_1)|} \quad (9)$$

The liquid profile in the expanding part is illustrated in Figure 17.

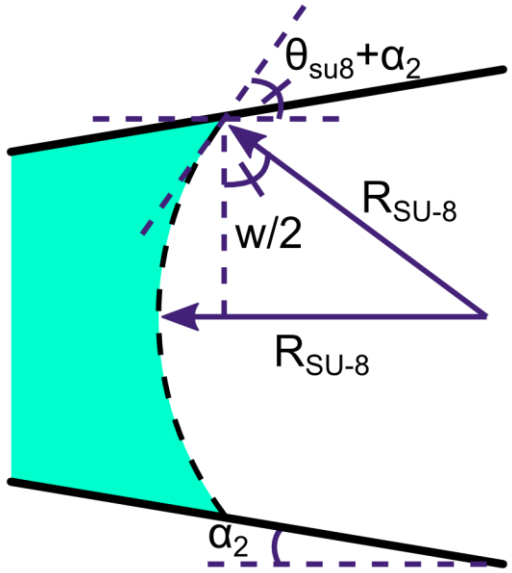

Figure 17: Liquid profile in an expanding channel

The radius of curvature is described by

$$R_{SU-8} = \frac{w}{-2\cos(\theta_{SU-8} + \alpha_2)}. \quad (10)$$

3.4 Contact angle vs. applied voltage in a parallel plate EWOD configuration

The asymmetric parallel plate EWOD configuration is illustrated in Figure 18.

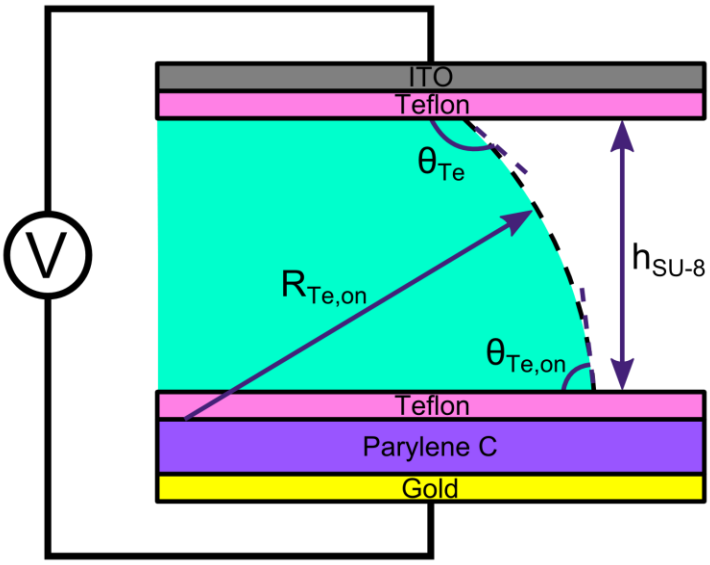

Figure 18: Liquid profile with an applied voltage

A 3-10 μm thick Parylene C layer is coated to the bottom plate as the dielectric. Then a thin layer of Teflon (about 100-200 nm thick) is coated to both the top and bottom plates to provide better hydrophobicity. The Parylene C and Teflon combination is a common choice in EWOD devices and has been utilized in many successful devices [33], [35], [36]. The relative dielectric constants of Parylene C is 3.1 (Specialty Coating Systems) and the relative dielectric constant of Teflon-AF 2400 is 2.1 (DuPont).

In this configuration, the capacitance across the Teflon layer at the top plate is much higher than the total capacitance across the Teflon and Parylene C layer at the bottom plate. Assuming that the liquid is conductive and there is no voltage drop across the liquid, the voltage drop across the Teflon layer is much lower (e.g. if 200 V is applied to a device with 100 nm thick Teflon and 6.2 um thick Parylene layers the voltage across the top and bottom layer would be 4.5 V and 195.5 V, respectively) and the contact angle change at the top when a voltage is applied is minimal and can be neglected. The radius of curvature of the liquid in contact with the Teflon layers when the voltage is turned on is

$$R_{Te,on} = \frac{h_{SU-8}}{-\left[\cos(\theta_{Te}) + \cos\left(\theta_{Te,on}\right)\right]}. \quad \textbf{(11)}$$

The contact angle change between the liquid and the Parylene and Teflon coated layer was measured using a contact angle tool (Attension Theta) on a droplet sandwiched between plates of the same configuration as in Figure 18. In these experiments, the sample is coated with 6.3 μm Parylene-C and 100 nm thick Teflon. Microscope slides that are 1 mm thick are used as spacers. The contact angle as a function of voltage is plotted in Figure 19. The theoretical analysis is based on the Lippmann-Young equation (equation (4)).

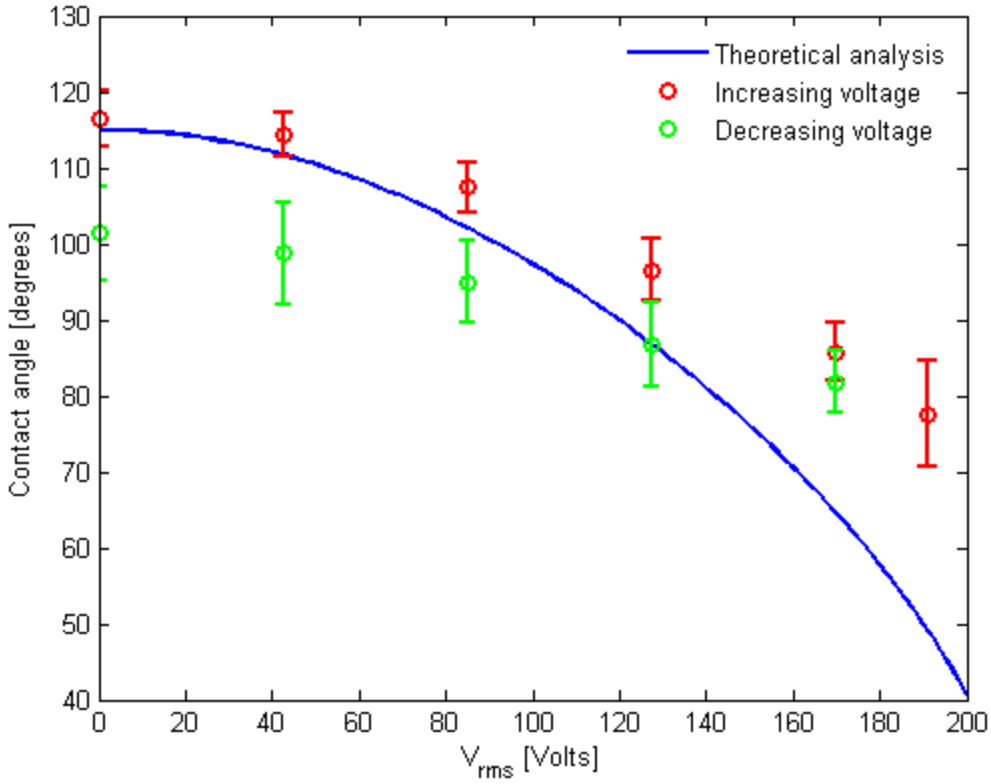

Figure 19: Contact angle vs. applied voltage

As shown on the graph in Figure 19, the bottom Teflon coating becomes more hydrophilic with an increasing voltage. At low voltages the experimental result is similar to the theoretical contact angle. At high voltages the contact angle deviates from the theoretical analysis. This is a common effect in EWOD known as the contact angle saturation [42]. After the voltage is reduced to zero, due to hysteresis, the contact angles return to a value that is lower than the initial value. An applied voltage at V_{rms} = 170 V is required to cause a contact angle change of approximately 20°.

If an identical dielectric layer is coated onto both the top and bottom plates of the device, half of the total voltage will be distributed across each layer and both the top and bottom would result in a contact angle change. Using the measured contact angle change at different applied voltages, the radius of curvature of the resulting liquid interface is calculated using equation (11). As shown in Table 3, within the working voltage range of this device, the asymmetric configuration can give a higher radius of curvature change under the same total applied voltage.

Table 3: Radius of curvature change in parallel plate EWOD configurations

	Symmetrical configuration (Two layers of Parylene C)		***Asymmetric configuration (one layer of Parylene C)***	
Total V	**θ at both top and bottom**	**R [μm]**	**θ at bottom**	**R [μm]**
0 V	115°	101	115°	101
40 V	115°	102	114°	102
60 V	115°	102	111°	108
80 V	114°	103	108°	116
100 V	113°	108	103°	130
120 V	111°	116	98°	150
140 V	110°	125	93°	177
160 V	108°	136	88°	217
180 V	106°	154	82°	305

The contact angle change was also recorded for frequencies between 1 to 10 kHz. No significant differences were observed between different frequencies. The data is shown in Figure 20.

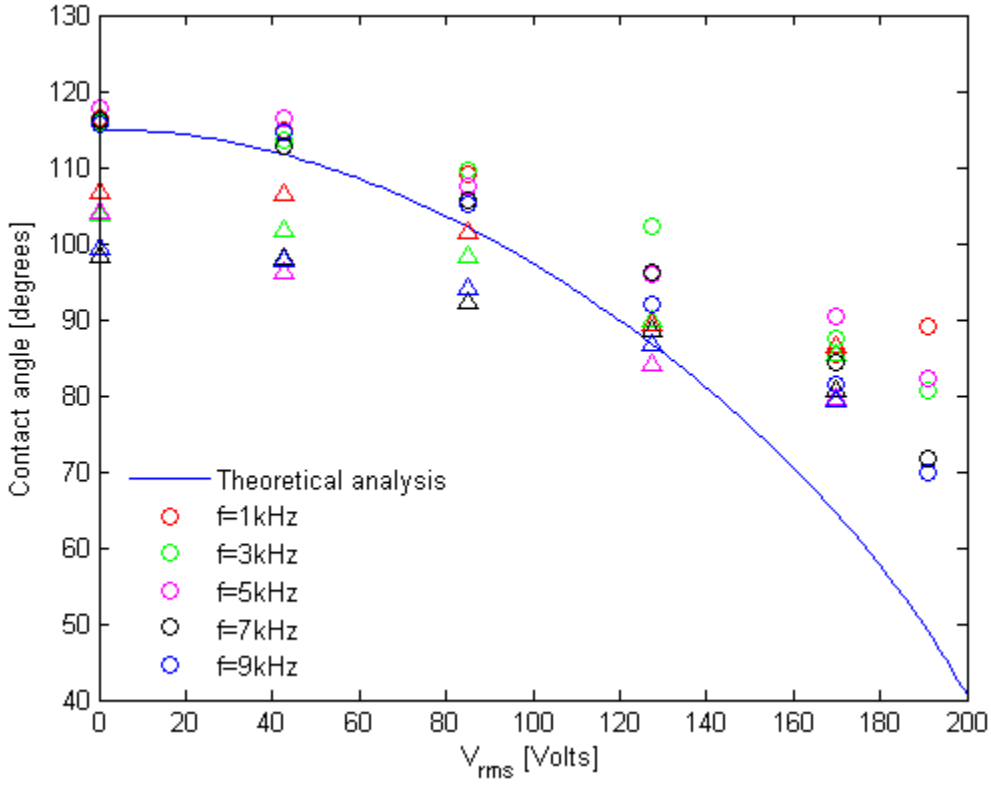

Figure 20: Contact angle at different frequencies; circles represent data for increasing voltages and triangles represent data for decreasing voltages

3.5 Pressure drop profile across the wedged channel

The Laplace pressure profile (equation (5)) as the liquid flows towards the carrier channel is plotted against the contact line and meniscus position in Figure 21. As shown on the graphs, when the liquid reaches the junction, it is pinned there and an increasing amount of pressure is required to move the meniscus towards the carrier channel. The graph in Figure 21 (b) represents the Laplace pressure as the meniscus moves towards the carrier channel with the contact line

being pinned at the junction. The barrier pressure, the maximum point in Figure 21 (b), represents the pressure required to push the liquid to the point where the liquid wets the side walls of the carrier channel for the first time. At this point, the contact angle between the liquid and the side walls of the carrier channel equals the static contact angle between the liquid and SU-8. As mentioned before, the static contact angle for SU-8 is measured to be 73° - 78° on SU-8 3050 using a contact angle tool (Attention Theta). However, the static contact angle of SU-8 inside channels of fabricated chips was measured to be 35° - 65° by identifying the curvature of best fit for the liquid interface. The value of the static SU-8 contact angle is different for different chips and is measured using the radius of curvature of the liquid at rest inside the channel. The static contact angle in bonded chips is lower than that on SU-8 surfaces likely as a result of the surface roughness at the SU-8 channel walls. A pressure drop above the barrier pressure would cause the liquid continuously flow into the carrier channel. This pressure barrier allows liquid to be easily stopped near the junction at a range of applied pressures.

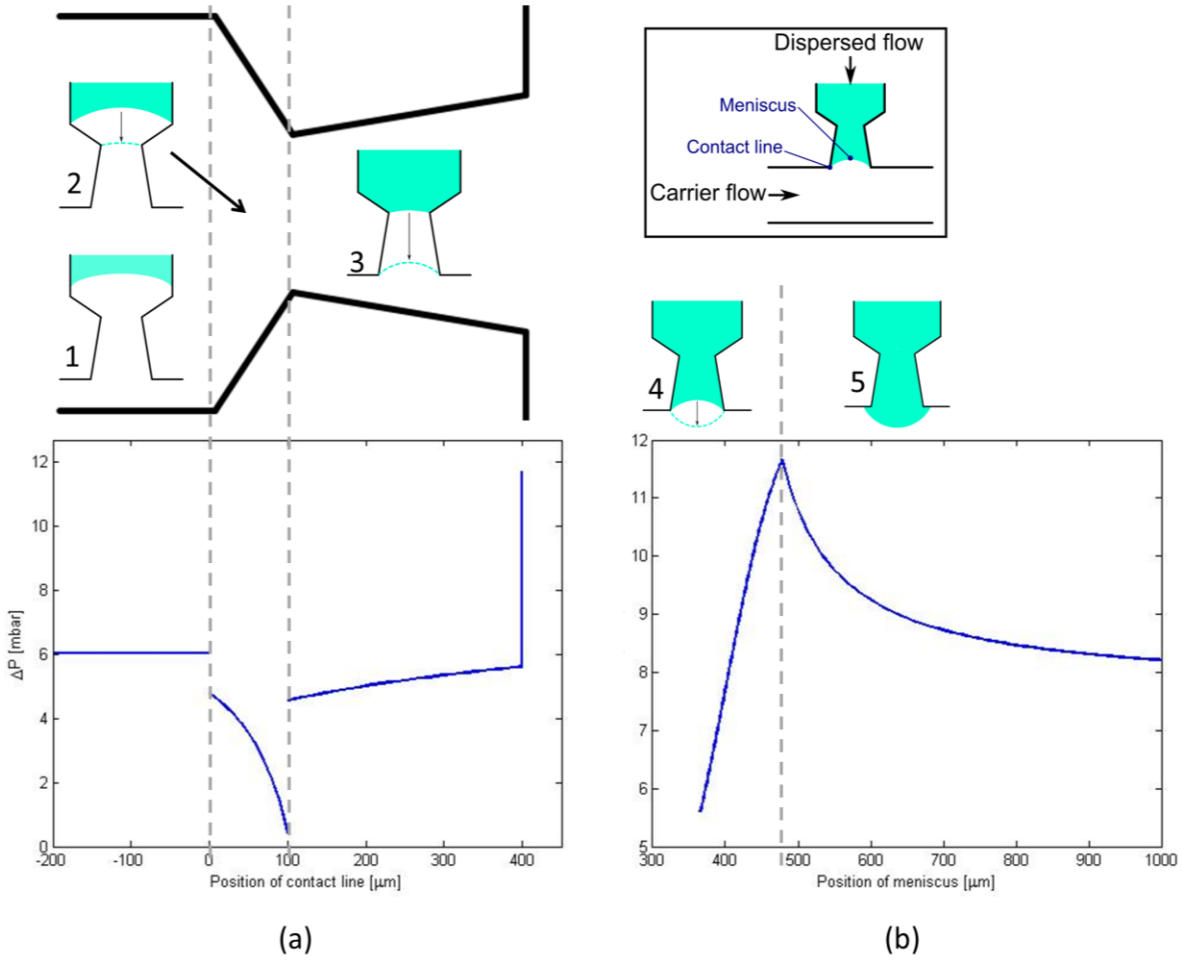

Figure 21: Calculated Laplace pressure profile as liquid moves towards the junction as a function of (a) the contact line and (b) the meniscus

When the electrode is turned on, the contact angle between the liquid and the bottom plate of the device is reduced, which leads to a larger radius of curvature $R_{Te,on}$, and as a result the Laplace pressure is reduced. Figure 22 shows the Laplace pressure change as the contact angle is reduced from 115° to 85° when the electrode is turned on. When the applied pressure is below the barrier pressure when the electrode is off but above the barrier pressure when the electrode is on, the

liquid will stop at the junction when the electrode is off and flow into the carrier channel when the electrode is on. This is the working range for the applied pressure for this device. Because there is a range of pressures that could work, even if different junctions have slight structural differences due to fabrication limitations, it should be possible to find a common applied pressure that would work for all the junctions in a chip with multiple junctions.

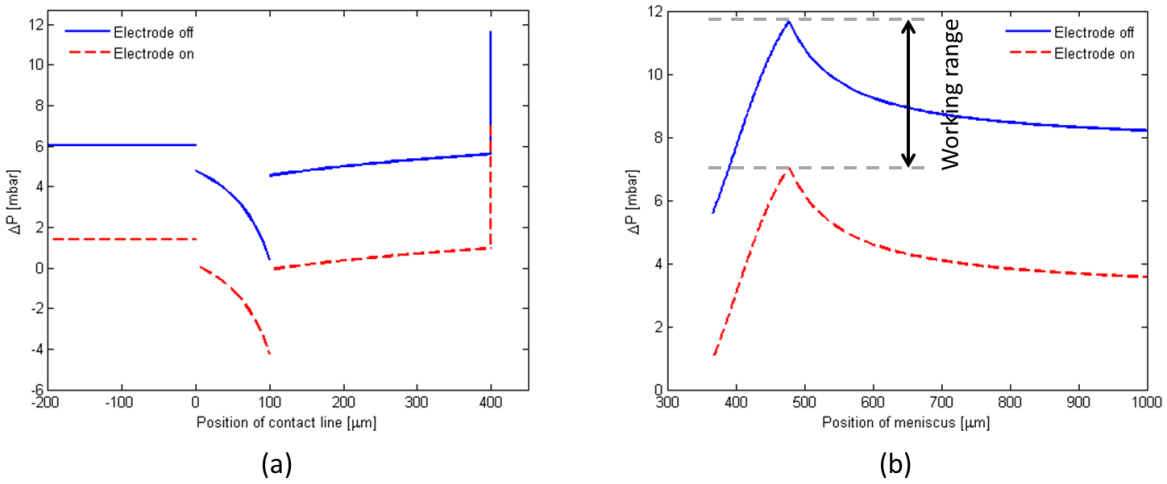

Figure 22: Laplace pressure change due to EWOD as a function of the location of (a) the contact line and (b) the meniscus

When the applied pressure is below the barrier pressure when the electrode is turned on, the liquid contact line and/or meniscus will move forward but will not start flowing when the electrode is turned on. This is shown in Figure 23.

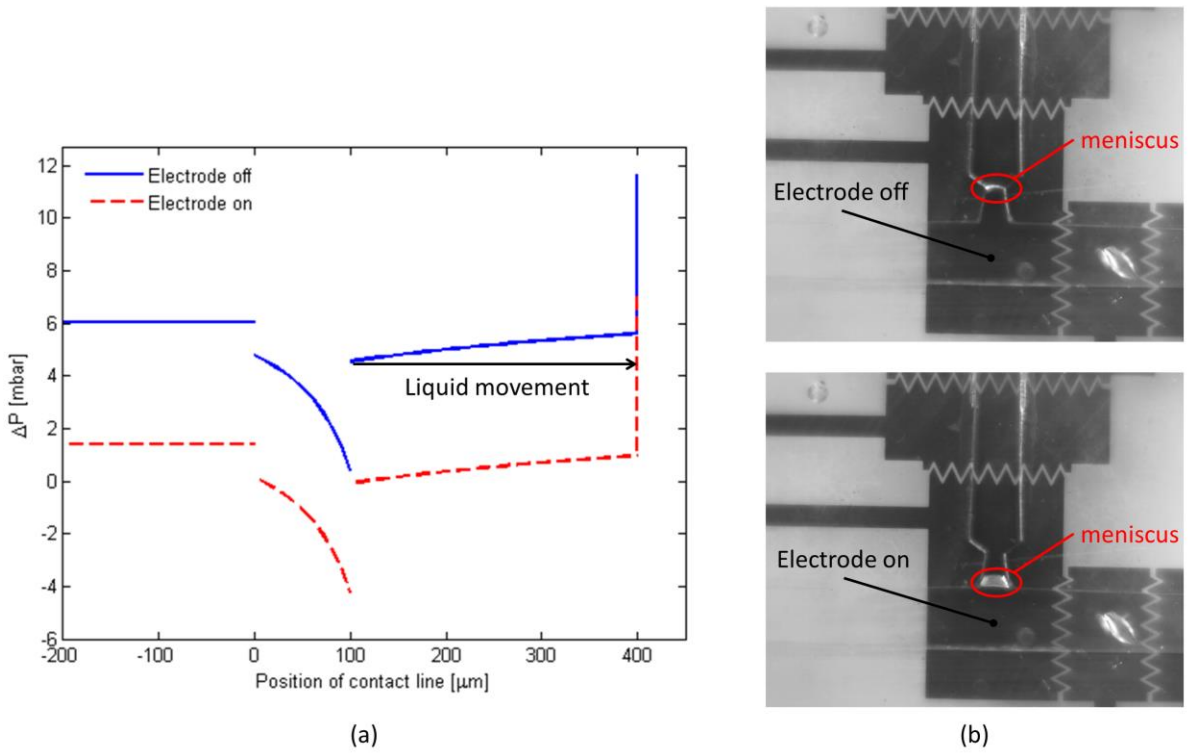

Figure 23: Liquid moving forward as a result of EWOD (a) graphical data (b) images of experiment results taken with a CMOS camera

Chapter 4: Experiments and discussion

4.1 Experimental apparatus and methodology

The experiment setup is shown in Figure 24. Two outlets of a pressure source (Fluigent MFCS-4C from Fluigent Inc, Lowell, Massachusetts) are driving the liquid and the air, which provides a constant applied pressure difference across the liquid interface in the dispersed channel. Tubing of appropriate size must be selected so the flow source can provide sufficient pressure. In case of the Fluidgent, Tygon formula R-3603 laboratory tubing I.D. 1/32 in. x O.D. 3/32 in. from United States Plastic Corp. (Lima, Ohio) was used. The liquid is 0.01 M KCl in distilled water. The pressure source driving the liquid is applied to the air above the liquid in a sealed 50 ml centrifuge bottle with an inner diameter of 29 mm. The change in height of the liquid in the bottle would change the hydrostatic pressure and therefore the pressure across the liquid interface. Using a droplet volume of $100 \cdot 10^{-12}$ m^3 (the maximum droplet size recorded was approximately $20 \cdot 10^{-12}$ m^3), liquid loss equivalent to more than 50 droplets will be required to cause a pressure change of 0.01 mbar. The number of droplets formed per experiment is always less than 50, which implies a pressure change per experiment of less than 0.01 mbar due to liquid loss and can be neglected.

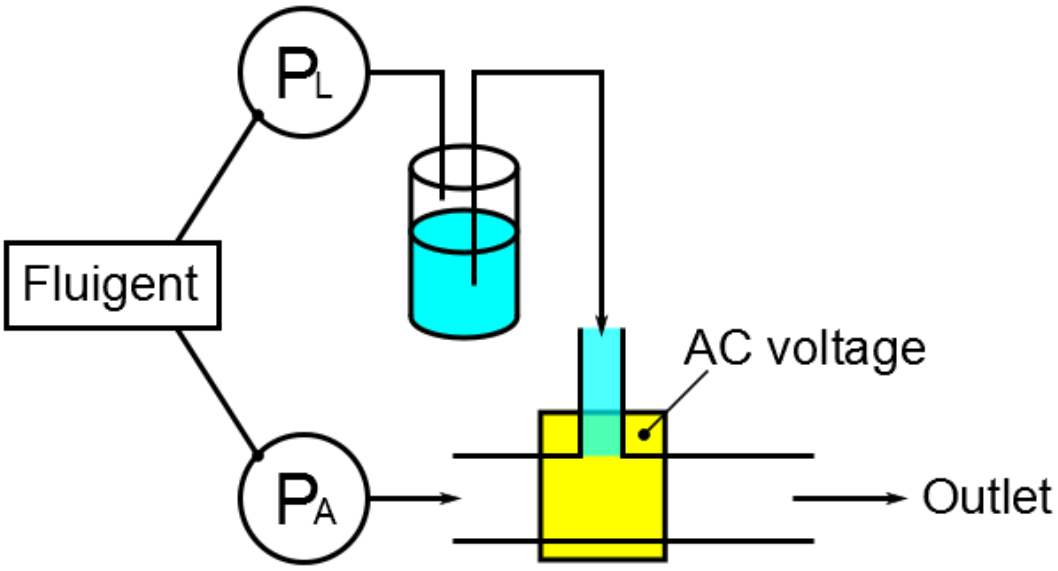

Figure 24: Experimental setup

The voltage is supplied by an arbitrary waveform generator (Agilent 33220A from Agilent Technologies, Santa Clara, California) connected to an amplifier (Trek Model 2210-CE high-voltage power amplifier from TREK Inc, Lockport, New York) with a gain of 100. The outputs of the amplifier are connected to the contact pad of the gold electrode and the ITO at the cover slide. Sinusoidal AC voltages ranging from V_{rms} = 130 V to 170 V at 5 kHz are applied. The channel dimensions are w_1 = 500 μm, w_2 = 200 μm, w_3 = 300 μm, h_1 = 100 μm, and h_2 = 300 μm for the experimental results in this chapter. A CMOS camera (EO-1312M ½" CCD Monochrome USB Camera from Edmund Optics Inc., Barrington, New Jersy) was placed above the junction of the chip to record images of the experiment.

Both AC and DC voltage could drive the electrowetting effect and cause a contact angle change. Initially experiments were done in DC voltage. Contact angle tests similar to the tests presented in section 3.4 were done and sufficient contact angle changes were observed under DC input.

However, when a DC voltage is applied to the electrode in the device, droplet formation did not take place; only liquid interface displacement was observed.

4.2 Static analysis

Several static experiments were done to verify the theoretical model. A pressure is applied to the liquid and another pressure is connected to both the air inlet and the outlet port of the chip to form a constant applied pressure difference across the liquid interface. Images of the liquid at different positions in the channel were taken and the applied pressures are calculated using the radii of curvature of the liquid interface. The static contact angle of SU-8 inside the channel is measured to be around 35° for the chip used in these experiments. The channel dimensions are w_1 = 700 µm, w_2 = 400 µm, w_3 = 500 µm, h_1 = 100 µm, and h_2 = 300 µm. As shown in Figure 25, the experiment data matches closely with the model.

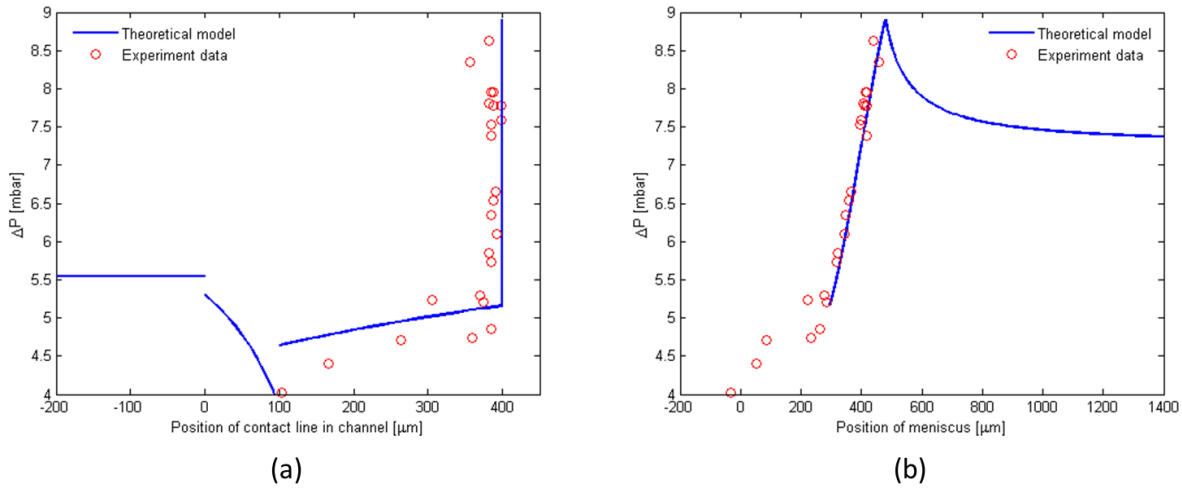

Figure 25: Static flow analysis where ΔP is calculated from liquid radius of curvature plotted as a function of (a) the contact line and (b) the meniscus

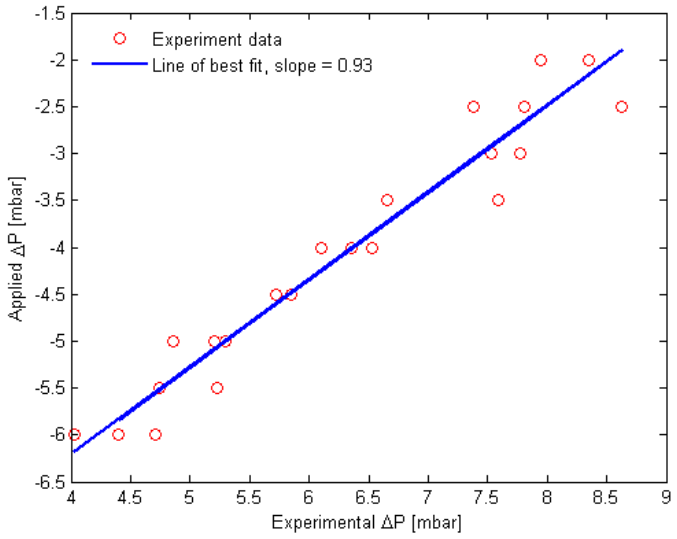

Figure 26: Applied pressure vs. experimental pressure

In Figure 26, the difference between the applied pressures ($\Delta P = P_L - P_A$) is plotted against the experimental Laplace pressure calculated from the radius of curvature measurements. The rates of change of the applied and experimental pressures are highly correlated. This supports the accuracy of the static model.

Using the same setup, a static test was conducted by applying a pressure difference at the liquid and recording the condition of the liquid interface before and after an AC voltage of V_{rms} = 170 V at f = 5 kHz. Since the applied pressures are maintained constant, the Laplace pressure

$$\Delta P = \gamma_{lg}\left(\frac{1}{R_{Te}} + \frac{1}{R_{SU-8}}\right) = \gamma_{lg}\left(\frac{1}{R_{Te,on}} + \frac{1}{R_{SU-8,on}}\right) \quad (12)$$

before and after the voltage is applied should be constant. From equation (12), the radius of curvature when the voltage is applied is

$$R_{Te.on} = \left(\frac{1}{R_{Te}} + \frac{1}{R_{SU-8}} - \frac{1}{R_{SU-8.on}}\right)^{-1}, \quad (13)$$

where $R_{SU\text{-}8,on}$ is the radius of curvature that the liquid form with the SU-8 surfaces after the voltage is applied. R_{Te} can be calculated from the static contact angle of Teflon. $R_{SU\text{-}8}$ and $R_{SU\text{-}8,on}$ were found using captured images. Using equations (11) and (13), the static contact angle of Teflon after a voltage is applied ($\theta_{Te,on}$) was calculated to be 87° with a standard deviation of 5.8°. The static contact angle of the SU-8 channel walls was measured to be 55°. Using these parameters, the data was plotted with the theoretical model in Figure 27. The applied pressures are calculated from the radii of curvature when the electrode is off. Data pairs without an 'On' location indicate the liquid has filled the main channel. As shown in Figure 27, when the applied pressure is above the barrier pressure of the 'On' curve, liquid will fill the main channel when the electrode is turned on. Otherwise it will just move forward.

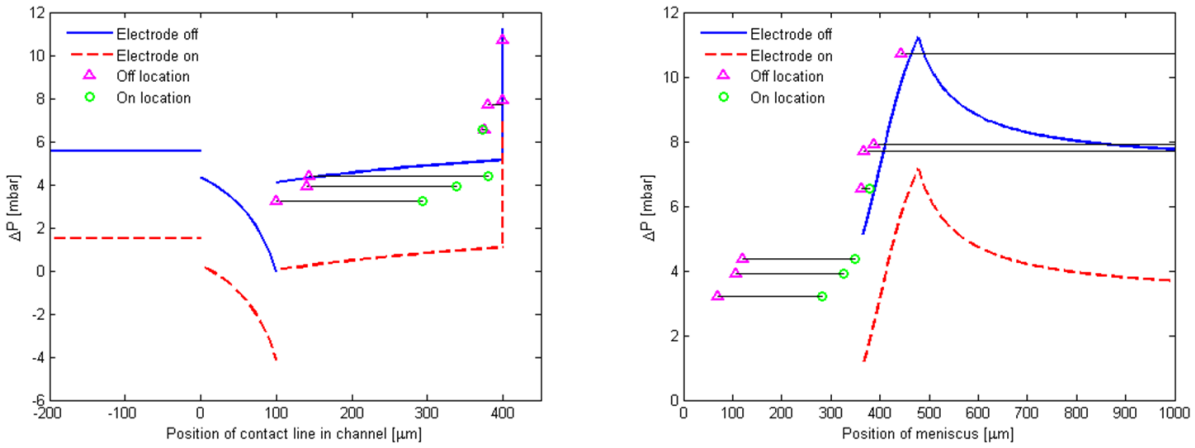

Figure 27: Static data (data points) vs. theoretical model (line) as a function of (a) the contact line and (b) the meniscus

4.3 Dynamic flow with applied voltage

The plots in Figure 28 show a comparison between dynamic test results and the static model presented in Chapter 3. The locations and radii of curvature of the liquid interface before and after applying an AC voltage of V_{rms} = 130, 150, or 170 V are recorded. The SU-8 contact angle was measured to be 50° and the Teflon contact angle when the voltage is applied is calculated to be 82° with a standard deviation of 4.5°. The position of the contact line and the position of the meniscus in Figure 28 before and after applying V_{rms} = 170 V are connected by a straight line. If the liquid continues to flow into the carrier channel to form droplets, then the data is represented as a straight line without an end point. As shown on the graphs, the dynamic data matches with the static model closely.

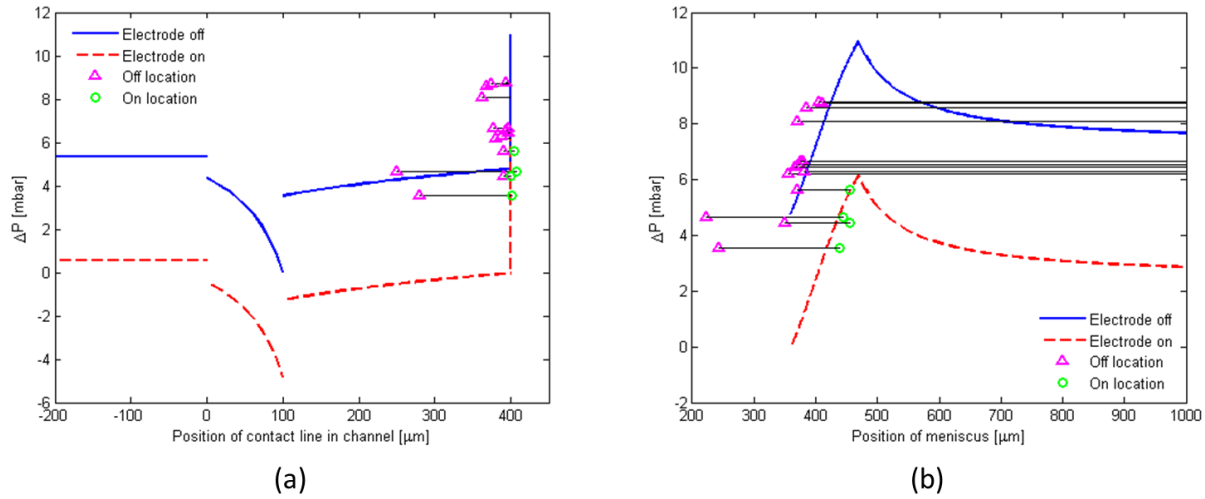

Figure 28: Location of the (a) contact line and (b) meniscus in dynamic flow tests with an applied voltage

4.4 Droplet formation frequency

Selected frames showing how droplets are formed in the device are shown in Figure 29. It was observed that droplets formed in the device do not extend to the opposite end of the carrier

channel. The droplets are attached to the SU-8 side wall as they flow toward the output. Droplet size was estimated using the area covered by the meniscus inside the carrier channel before the droplet breakup. Similar to the experimental results from the study done by Oskooei *et al.*, aliquots formed in this system show some variability in size [14]. The sizes of the droplets formed in this device are around 8-18 nL.

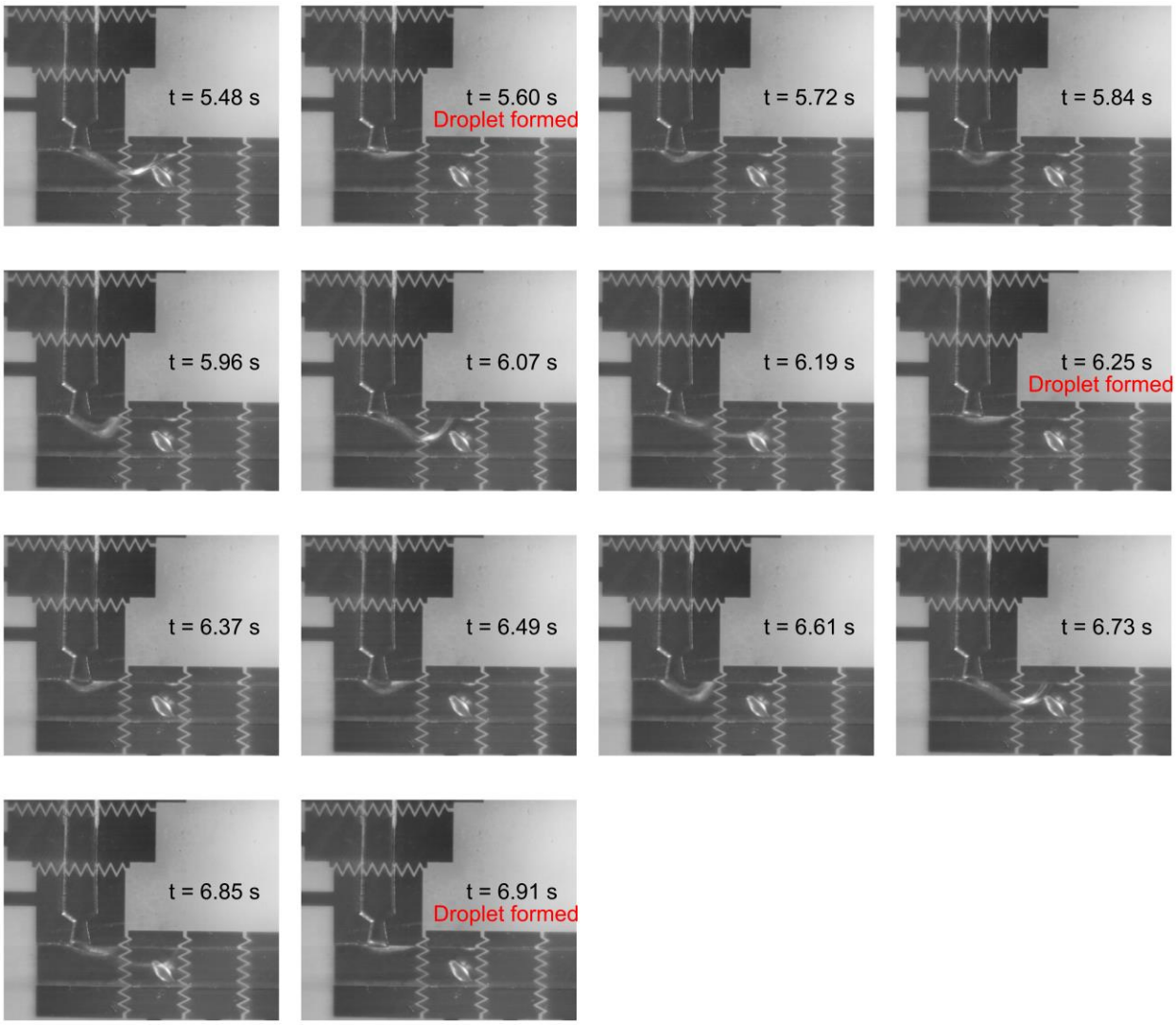

Figure 29: Selected frames showing the formation of droplets

The frequencies of droplet formation at different applied pressures and voltages were recorded by taking the inverse of the time between the formations of two droplets in the experiments. The mean frequency and standard deviations as a function of applied pressure are plotted in Figure 30. The applied pressures are calculated using the radii of curvature of the liquid before the voltage is applied. As shown on the graph, higher applied pressures and/or applied voltages will result in higher droplet formation frequencies. This suggests that frequency can be controlled digitally by varying the applied voltage, a feature that is not possible in the conventional flow rate driven T-junction mechanism.

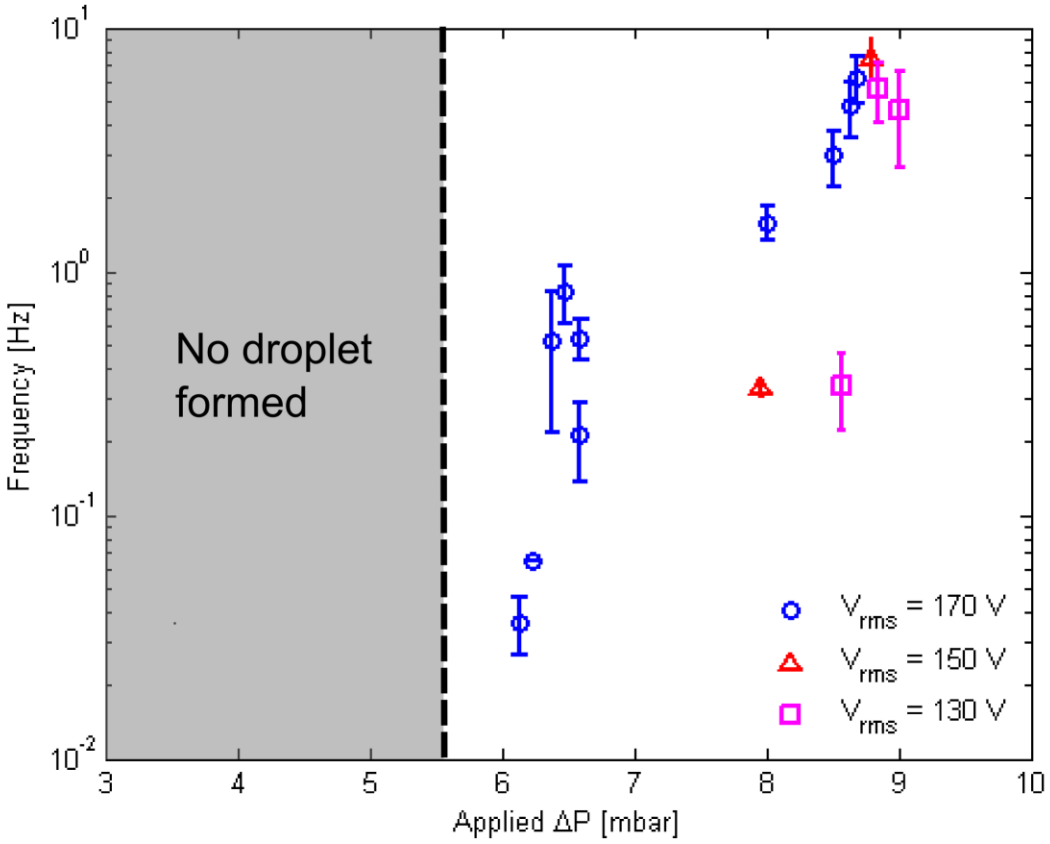

Figure 30: Droplet formation frequency

Chapter 5: Conclusions and future work

A device that combines a microfluidic T-junction with EWOD to form air separated aliquots on demand was designed and fabricated. A double wedged junction was incorporated to create a barrier pressure at the junction so that the position of the meniscus in the dispersed channel can be controlled by the applied pressures. When the liquid is held near the junction with an applied pressure that is within the range of the working pressure, applying or removing a voltage at the electrode can start or stop liquid flow, respectively. Using this mechanism, air separated aliquots that are otherwise difficult to form stably can be formed at a microfluidic T-junction. Experimental results matched closely with theoretical expectations and demonstrated that the droplet formation frequency is dependent on the applied pressure and there are trends showing that it could be controlled by varying the magnitude of the applied voltage. This new droplet formation mechanism can act as a digital valve for multi-material lab-on-a-printer inkjet printing platforms.

In the current system, the SU-8 channel walls are hydrophilic with a static contact angle that could vary from chip to chip. Hydrophilic walls are not suitable for a multi-material chip because droplets could flow into adjacent dispersed channels as they flow towards the output. If a uniform hydrophobic coating with known thickness and surface properties can be coated onto the fabricated channels, the surface properties of the channel walls can be standardized. With hydrophobic channel walls, it is unlikely that droplets formed will flow into other dispersed channels.

Aliquots formed in the current system do span the carrier channel. This could be because the carrier channel is too wide. As a result, the generated droplets are being dragged towards the output by the air flow due to the shear force at the surface of the droplets. Aliquots that span across the channel will be transported towards the output with the air spacer in a plug-like fashion instead of being dragged along, which could result in a faster and more stable flow. In the current geometry, the width of the carrier channel is designed to be twice the width of the opening of the dispersed channel. Channels with different width ratios should be studied.

Dielectric thickness plays an important role in this device. By using a thinner dielectric layer, a lower actuation voltage would be needed. However, a dielectric layer that is too thin would lead to more frequent dielectric breakdown. It was found that devices with 3 μm thick Parylene layers would experience breakdown quite frequently and therefore this thickness is not suitable. In the current devices, Parylene C thickness is targeted to be around 5-6 μm. But dielectric breakdown was still observed in many fabricated devices after some experiments. Improvements to the dielectric layer fabrication technique that would lead to a more durable layer could greatly improve the performance and durability of the device.

Bibliography

[1] J. Tian, K. Ma, and I. Saaem, "Advancing high-throughput gene synthesis technology," *Mol. Biosyst.*, vol. 5, no. 7, pp. 714–722, Jun. 2009.

[2] L. Mere, T. Bennett, P. Coassin, P. England, B. Hamman, T. Rink, S. Zimmerman, and P. Negulescu, "Miniaturized FRET assays and microfluidics: key components for ultra-high-throughput screening," *Drug Discov. Today*, vol. 4, no. 8, pp. 363–369, Aug. 1999.

[3] J. R. Busch, C. Sielmann, G. Man, D. Tsan, K. Walus, and B. Stoeber, "Inkjet printed all-polymer flexural plate wave sensors," in *2012 IEEE 25th International Conference on Micro Electro Mechanical Systems (MEMS)*, 2012, pp. 571–574.

[4] E. R. Lee, *Microdrop Generation*, 1 edition. Boca Raton: CRC Press, 2002.

[5] D. L. Chen and R. F. Ismagilov, "Microfluidic cartridges preloaded with nanoliter plugs of reagents: an alternative to 96-well plates for screening," *Curr. Opin. Chem. Biol.*, vol. 10, no. 3, pp. 226–231, Jun. 2006.

[6] K. Churski, P. Korczyk, and P. Garstecki, "High-throughput automated droplet microfluidic system for screening of reaction conditions," *Lab. Chip*, vol. 10, no. 7, pp. 816–818, Apr. 2010.

[7] L. Li, M. Saedan, W. Feng, J. Y. H. Fuh, Y. S. Wong, H. T. Loh, S. C. H. Thian, S. T. Thoroddsen, and L. Lu, "Development of a multi-nozzle drop-on-demand system for multi-material dispensing," *J. Mater. Process. Technol.*, vol. 209, no. 9, pp. 4444–4448, May 2009.

[8] J. Sun, R. Yang, K. K. Tan, J. Y. H. Fuh, Y. S. Wong, and J. H. Ng, "Performance characterization of drop-on-demand micro-dispensing system with multi-printheads," *Microsyst. Technol.*, vol. 16, no. 12, pp. 2087–2097, Dec. 2010.

[9] E. Um, M. E. Rogers, and H. A. Stone, "Combinatorial generation of droplets by controlled assembly and coalescence," *Lab. Chip*, vol. 13, no. 23, pp. 4674–4680, Oct. 2013.

[10] V. Linder, S. K. Sia, and G. M. Whitesides, "Reagent-Loaded Cartridges for Valveless and Automated Fluid Delivery in Microfluidic Devices," *Anal. Chem.*, vol. 77, no. 1, pp. 64–71, 2004.

[11] A. K. Au, H. Lai, B. R. Utela, and A. Folch, "Microvalves and Micropumps for BioMEMS," *Micromachines*, vol. 2, no. 2, pp. 179–220, May 2011.

[12] K. W. Oh and C. H. Ahn, "A review of microvalves," *J. Micromechanics Microengineering*, vol. 16, no. 5, p. R13, May 2006.

[13] W. Gu, X. Zhu, N. Futai, B. S. Cho, and S. Takayama, "Computerized microfluidic cell culture using elastomeric channels and Braille displays," *Proc. Natl. Acad. Sci. U. S. A.*, vol. 101, no. 45, pp. 15861–15866, Nov. 2004.

[14] S. A. Kazemi Oskooei and D. Sinton, "Partial wetting gas-liquid segmented flow microreactor," *Lab. Chip*, vol. 10, no. 13, pp. 1732–1734, Jul. 2010.

[15] P. Garstecki, M. J. Fuerstman, H. A. Stone, and G. M. Whitesides, "Formation of droplets and bubbles in a microfluidic T-junction—scaling and mechanism of break-up," *Lab. Chip*, vol. 6, no. 3, pp. 437–446, Feb. 2006.

[16] J. H. Xu, S. W. Li, J. Tan, Y. J. Wang, and G. S. Luo, "Preparation of highly monodisperse droplet in a T-junction microfluidic device," *AIChE J.*, vol. 52, no. 9, pp. 3005–3010, Sep. 2006.

[17] A.-B. Wang, I.-C. Lin, Y.-W. Hsieh, W.-P. Shih, and G.-W. Wu, "Effective pressure and bubble generation in a microfluidic T-junction," *Lab. Chip*, vol. 11, no. 20, pp. 3499–3507, Oct. 2011.
[18] F. Malloggi, H. Gu, A. G. Banpurkar, S. A. Vanapalli, and F. Mugele, "Electrowetting -- A versatile tool for controlling microdrop generation," *Eur. Phys. J. E*, vol. 26, no. 1–2, pp. 91–96, May 2008.
[19] J. H. Xu, S. W. Li, Y. J. Wang, and G. S. Luo, "Controllable gas-liquid phase flow patterns and monodisperse microbubbles in a microfluidic T-junction device," *Appl. Phys. Lett.*, vol. 88, no. 13, p. 133506, Mar. 2006.
[20] F. Trachsel, A. Günther, S. Khan, and K. F. Jensen, "Measurement of residence time distribution in microfluidic systems," *Chem. Eng. Sci.*, vol. 60, no. 21, pp. 5729–5737, Nov. 2005.
[21] T. Cubaud, U. Ulmanella, and C.-M. Ho, "Two-phase flow in microchannels with surface modifications," *Fluid Dyn. Res.*, vol. 38, no. 11, p. 772, Nov. 2006.
[22] A. Günther, M. Jhunjhunwala, M. Thalmann, M. A. Schmidt, and K. F. Jensen, "Micromixing of Miscible Liquids in Segmented Gas−Liquid Flow," *Langmuir*, vol. 21, no. 4, pp. 1547–1555, Feb. 2005.
[23] A. Günther, S. A. Khan, M. Thalmann, F. Trachsel, and K. F. Jensen, "Transport and reaction in microscale segmented gas–liquid flow," *Lab. Chip*, vol. 4, no. 4, pp. 278–286, Jul. 2004.
[24] S. K. Cho, H. Moon, and C.-J. Kim, "Creating, transporting, cutting, and merging liquid droplets by electrowetting-based actuation for digital microfluidic circuits," *J. Microelectromechanical Syst.*, vol. 12, no. 1, pp. 70–80, Feb. 2003.
[25] S. W. Walker and B. Shapiro, "Modeling the fluid dynamics of electrowetting on dielectric (EWOD)," *J. Microelectromechanical Syst.*, vol. 15, no. 4, pp. 986–1000, Aug. 2006.
[26] J. Lee, H. Moon, J. Fowler, T. Schoellhammer, and C.-J. Kim, "Electrowetting and electrowetting-on-dielectric for microscale liquid handling," *Sens. Actuators Phys.*, vol. 95, no. 2–3, pp. 259–268, Jan. 2002.
[27] T. B. Jones, "An electromechanical interpretation of electrowetting," *J. Micromechanics Microengineering*, vol. 15, no. 6, p. 1184, Jun. 2005.
[28] W. C. Nelson and C.-J. "CJ" Kim, "Droplet Actuation by Electrowetting-on-Dielectric (EWOD): A Review," *J. Adhes. Sci. Technol.*, vol. 26, no. 12–17, pp. 1747–1771, 2012.
[29] F. Mugele and J. Buehrle, "Equilibrium drop surface profiles in electric fields," *J. Phys. Condens. Matter*, vol. 19, no. 37, p. 375112, Sep. 2007.
[30] "Micro and Nanoscale Fluid Mechanics Transport in Microfluidic Devices | Thermal-fluids engineering | Cambridge University Press." [Online]. Available: http://www.cambridge.org/us/academic/subjects/engineering/thermal-fluids-engineering/micro-and-nanoscale-fluid-mechanics-transport-microfluidic-devices. [Accessed: 28-Aug-2014].
[31] D. Chatterjee, B. Hetayothin, A. R. Wheeler, D. J. King, and R. L. Garrell, "Droplet-based microfluidics with nonaqueous solvents and solutions," *Lab. Chip*, vol. 6, no. 2, pp. 199–206, Jan. 2006.

[32] M. J. Jebrail, H. Yang, J. M. Mudrik, N. M. Lafrenière, C. McRoberts, O. Y. Al-Dirbashi, L. Fisher, P. Chakraborty, and A. R. Wheeler, "A digital microfluidic method for dried blood spot analysis," *Lab. Chip*, vol. 11, no. 19, pp. 3218–3224, Sep. 2011.
[33] V. Srinivasan, V. K. Pamula, and R. B. Fair, "Droplet-based microfluidic lab-on-a-chip for glucose detection," *Anal. Chim. Acta*, vol. 507, no. 1, pp. 145–150, Apr. 2004.
[34] S. C. C. Shih, N. S. Mufti, M. D. Chamberlain, J. Kim, and A. R. Wheeler, "A droplet-based screen for wavelength-dependent lipid production in algae," *Energy Environ. Sci.*, vol. 7, no. 7, pp. 2366–2375, Jun. 2014.
[35] N. Vergauwe, D. Witters, F. Ceyssens, S. Vermeir, B. Verbruggen, R. Puers, and J. Lammertyn, "A versatile electrowetting-based digital microfluidic platform for quantitative homogeneous and heterogeneous bio-assays," *J. Micromechanics Microengineering*, vol. 21, no. 5, p. 054026, May 2011.
[36] M. J. Schertzer, R. Ben-Mrad, and P. E. Sullivan, "Using capacitance measurements in EWOD devices to identify fluid composition and control droplet mixing," *Sens. Actuators B Chem.*, vol. 145, no. 1, pp. 340–347, Mar. 2010.
[37] S. Morishita, M. Kubota, and Y. Mita, "Integration of EWOD pumping device in deep microfluidic channels using a three-dimensional shadowmask," in *2012 IEEE 25th International Conference on Micro Electro Mechanical Systems (MEMS)*, 2012, pp. 1045–1048.
[38] J. Jenkins and C. J. Kim, "Generation of Pressure by EWOD-Actuated Droplets," in *Solid-State Sensor, Actuator and Microsystems Workshop Technical Digest*, Hilton Head Island, SC, pp. 145–148.
[39] R. P. von Metzen and T. Stieglitz, "The effects of annealing on mechanical, chemical, and physical properties and structural stability of Parylene C," *Biomed. Microdevices*, vol. 15, no. 5, pp. 727–735, Oct. 2013.
[40] S.-W. Youn, H. Goto, S. Oyama, M. Takahashi, and R. Maeda, "Control of Parameters Influencing the Thermal Imprint of Parylene/Silicon," *Jpn. J. Appl. Phys.*, vol. 46, no. 9S, p. 6363, Sep. 2007.
[41] S. G. Serra, A. Schneider, K. Malecki, S. E. Huq, and W. Brenner, "A simple bonding process of SU-8 to glass to seal a microfluidic device," in *In Proc.*, Borovets, 2007, pp. 43–6.
[42] A. Quinn, R. Sedev, and J. Ralston, "Contact Angle Saturation in Electrowetting," *J. Phys. Chem. B*, vol. 109, no. 13, pp. 6268–6275, 2005.

Appendices

Appendix A: Bonder parts

The following list is the parts needed to assemble the bonder in Figure 10.

- Thorlabs MB4A - Aluminum Breadboard, 4.5" x 4.5" x 1/2", 1/4"-20 Threaded
- Thorlabs RS2 - Ø1" Pillar Post Extension, Length=2"
- Thorlabs RS1M - Ø25.0 mm Pillar Post Spacer, Thickness = 1 mm
- Thorlabs RLA0600 - Imperial Dovetail Optical Rail, 6"
- Thorlabs BA1 - Mounting Base, 1" x 3" x 3/8"
- Thorlabs BA2 - Mounting Base, 2" x 3" x 3/8"
- McMaster-Carr Heat-Resistant Borosilicate Glass Square, 5/8" Thick, 3" x 3" Part number: 8476K137